POLITECNICO DI TORINO

Dipartimento di Ingegneria Meccanica ed Aerospaziale

Corso di Laurea Magistrale in Ingegneria Aerospaziale

Self-excited oscillations in collapsible tubes

Relatore:
Prof. S. Scarsoglio

Relatore esterno:
Prof. V. Raghav

Candidato:
Nicola Francescato

Anno accademico 2022/2023

Contents

Chapter 1

Introduction

1.1 Collapsible tubes

Collapsible tubes are an important category of ducts that play a vital role in biofluid dynamics and biomedical engineering. A collapsible tube is essentially a tube with elastic walls that conveys one fluid, where the pressure inside the tube can differ from the pressure outside. According to this pressure difference, the shape of the collapsible tube can change.

Examples of collapsible tubes found in the human body include blood vessels, pulmonary airways, urethra, Eustachian tube, vocal chords, as well as devices such as amplifiers, switches, and logic units. This explains why during the last decades research have been done about collapsible tubes. A deeper comprehension of the collapsible tubes has direct impact in the creation of diagnostic and therapeutic devices, like prosthetic vocal cords, prosthetic heart devices or vascular diagnosis by pressurizing cuffs.

Studying the properties of collapsible tubes allows us to understand how diseases such as COPD (Chronic Obstructive Pulmonary Disease) cause lung collapse during expiration, which in turn enables us to work towards mitigating their impact.
It is worth noting that COPD is presently the fourth leading cause of death in the United States. COPD is often caused by exposure to irritants such as smoking or air pollution. Symptoms include shortness of breath, coughing, and chest tightness, which can lead to breathing-related problems.

The significance of understanding the mechanisms governing tube collapse is what motivated me to research collapsible tubes for my thesis. Specifically, my thesis is an experimental study that enables me to replicate several important aspects of collapsible tubes.
In experimental studies, a collapsible tube is typically approximated using the Starling Resistor model, shown in figure 1.1. This model consists of a collapsible tube with a constant cross-section, made from elastic material, and clamped between two rigid supports inside a pressure chamber. A fluid flows through the tube due to the difference between the pressure upstream (p^*_{up}) and downstream (p^*_{dn}) of the tube, with the pressure of the chamber (p^*_{ext}) being adjustable. Depending on the values of fluid dynamic variables, the collapsible tube can be either fully open, partially or totally collapsed, or oscillating (as explained in paragraph 2.4). While my thesis covers all three configurations, my focus is primarily on self-excited oscillations.

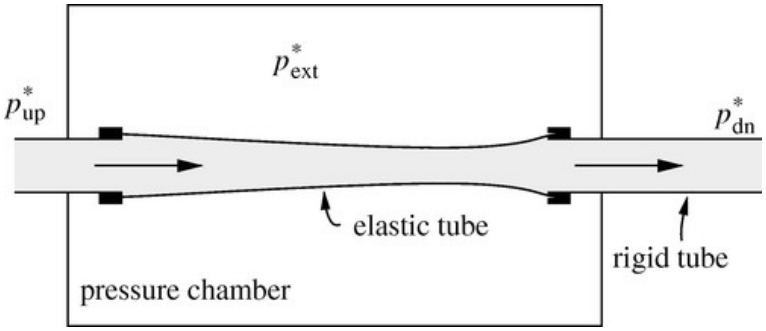

Figure 1.1: Starling Resistor model

This thesis is organized as follows: Chapter 2 provides an introduction to the most relevant properties of collapsible tubes, with a particular focus on their fluid dynamics; Chapter 3 describes the experimental setup and the manufacturing process of the tube, as well as the optical techniques that are used; Chapter 4 outlines the process of preparing for the experiment, including calibrations and setup preparation. The results of the experiments are presented in Chapter 5, and are discussed in Chapter 6. Finally, the main conclusions are presented in Chapter 7.

Chapter 2

Fluid dynamics of collapsible tubes

This chapter examines the key aspects of collapsible tubes, with a focus on the fluid dynamics that govern their behavior. To this end, we introduce the following variables:

- p_1: The pressure measured just upstream of the collapsible tube
- p_2: The pressure measured just downstream of the collapsible tube
- p_e: The pressure of the pressure chamber
- Q: The flow rate inside the collapsible tube

Typically, the pressure differentials are more important than their absolute values. For instance, the difference $p_{e2} = p_e - p_2$ is often of greater significance than either p_e or p_2 alone.

2.1 Tube Law

The shape of the collapsible tube is strongly related to the pressure difference between inside and outside of the tube. In fact, when the pressure difference is zero the tube is completely open but when the pressure chamber is pressurised the tube starts to change its shape: initially the tube starts to be elliptic and the cross sectional area of the tube decrease; after increasing the pressure again, the tube has the shape of a dumbbell.
This behavior is shown in figure 2.1, where the x-axis is the cross sectional area ratio $\alpha = A/A_0$ (where A_0 is the cross sectional area when $p_{int} = p_{ext}$) and y-axis is the intramural pressure, i.e. the pressure difference $p_{int} - p_{ext}$.
It is possible to notice that the collapse of the tube happens very rapidly when the pressure increases. Even if the diagram intramural pressure -Area ratio slightly changes with the tube properties as thickness or Young modulus, it is possible to define empirical laws, called the tube law:

$$p - p_e = P(\alpha) \tag{2.1}$$

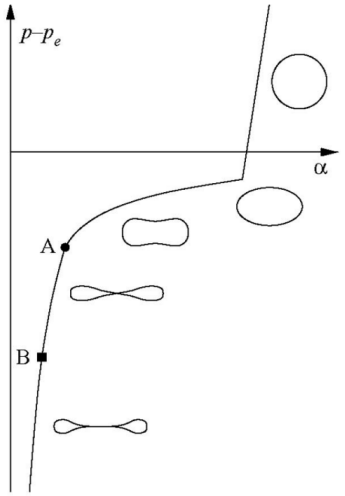

Figure 2.1: Behavior of the collapsible tube when the intramural pressure changes

2.2 Flow Limitation

One of the most relevant properties of the collapsible tubes is the flow limitation. This property is strictly connected to the elasticity of the tube, and it does not appear in the rigid tube at subsonic speed.
If it is considered a rigid tube of length L that contains a flow and a pressure difference Δp is applied between the ends of the tube, the flow rate Q inside the tube will be:

$$Q = \frac{\Delta p A^{1/2}}{8\pi\mu L} = \frac{\Delta p}{R} \tag{2.2}$$

Where μ is the dynamic viscosity of the fluid, and A is the cross-sectional area of the tube; R is the resistance of the tube and contains both properties of the tube and of the fluid. In this case there is a linear relationship between the flow rate and the pressure difference applied.
The previous law can not be applied to a collapsible tube: in fact, is it possible to see that when the Δp in increased, the flow rate increase until reaching a maximum. After that point, the flow rate becomes almost constant and independent from the driven pressure difference.

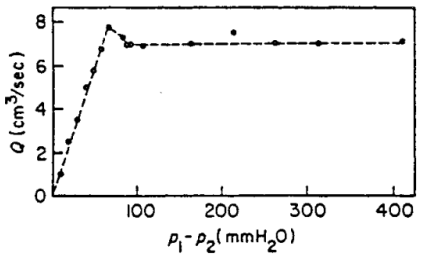

Figure 2.2: Flow limitation when $p_u - p_e = const$

When the flow limitation occurs, the resistance of the tube has not a steady value. The flow limitation occurs when the tube is partially collapsed.

2.3 Pressure waves velocity

Ideally, when a rigid pipe is perturbed (e.g., by applying pressure to the internal walls), the perturbation travels through the pipe at infinite velocity. In contrast, in a collapsible tube, the velocity of pressure wave perturbations can be defined. Shapiro [13] hypothesized the velocity for a 1D model as:

$$c^2 = \frac{A}{\rho}\frac{d(p - p_e)}{dA} \tag{2.3}$$

where A is the cross-sectional area of the collapsible tube, ρ the density of the fluid and $p - p_e$ is the local difference between the pressure inside and outside of the collapsible tube.
It is possible to notice that this velocity is similar to the velocity of small pressure perturbation in compressible flow $c^2 = \frac{d(p)}{d\rho}$.
Another analogy between the flow in a collapsible tube and a compressible flow is the importance of the ratios between the velocity of the flow and the velocity of pressure's perturbations.

$$M = u/c \tag{2.4}$$

$$S = u/c \tag{2.5}$$

Where M is the Mach number and S is defined as Shapiro number. When $S < 1$ the flow is subcritical, when $S = 1$ is critical and when $S > 1$ is supercritical.
The behavior of the flow changes drastically according to the value of the Shapiro's number: subcritical and supercritical flows have opposite characteristics. Cancelli [2] showed that self excited oscillations can be generated by supercritical flow.

2.4 Self excited oscillations

Another important property of the collapsible tube is the onset of self-excited oscillations. These oscillations arise because a portion of the flow kinetic energy is converted into kinetic energy of the collapsible tube wall [8]. During self-excited oscillations, pressure, flow rate, and cross-sectional area change periodically, and the throat moves downstream, opens, and then returns upstream. The oscillations exhibit strong hysteresis [3].

The reason why oscillations appear has not been found yet, even if a lot of experiments have been carried out during the last decades and several computational models have been presented. Oscillations can be divided into two main groups:

- Flutter oscillations. Those kind of oscillations appear when the inertia of the flow is negligible compared to the inertia of the walls of the collapsible tubes (i.e. with gas). The frequency of ths oscillations is high and it is possible to find stationary choke points.
- Milking oscillations. They happen when the fluid inertia is high and the wall inertia small. This case appears when the working fluid is a liquid

The Reynolds number when oscillations appear is different according to the thickness of the collapsible tube: thick tubes need higher Reynolds number (about 5000) than the thin ones (between 300<Re<500). Milking oscillations, that are the ones that are studied

in this thesis, can be divided also according to their period into [12]:

- Periodic: a main frequency of oscillations is clearly visible;
- Period-doubling: a second frequency appears, with a frequency that is the double of the main one;
- Quasi-periodic: even if it is possible to recognize a main frequency, some other spurious frequency are present;
- Chaotic: there is not a main frequency of oscillations;

Until now, research on the oscillations of collapsible tubes has mainly relied on experimental or computational fluid dynamics approaches. Wang's article [9] has been particularly instrumental in establishing experimental setups that induce self-excited oscillations by exploring various parameters, such as resistances or the height of the reservoir.
However, there has been no previous study that has endeavored to investigate both the shape of the collapsible tube and the flow field just downstream of it simultaneously. Although particle image velocimetry (PIV) has been applied to the study of velocity field in the past [4, 5] or other optical techniques to investigate the shape of the tube [7], this experiment represents the first effort to jointly investigate both the tube shape and the downstream flow field.

2.5 Dimensional analysis

To have a better understanding of the physical phenomenon, it was made a dimensional analysis, applying Buckingham's theorem.
Nine dimensional parameters were considered

$$f\left(u, D, \nu, E\left(\frac{t}{R}\right)^3 \frac{1}{12(1-v^2)}, \rho, p_{12}, p_{pe2}, L, t\right) = 0, \tag{2.6}$$

where u is the mean flow velocity inside the pipes, D the internal diameter of the pipe (and of the collapsible tube when non collapsed), ν the viscosity of the fluid, t the thickness of the collapsible tube, E the Young's modulus, v the Poisson ratio, ρ the density of the fluid and L the length of the collapsible tube.
It is important to notice that in the fourth parameter, instead of using only E, it was considered the stiffness parameter. From this point, the stiffness parameter will be written as:

$$K_s = E\left(\frac{t}{R}\right)^3 \frac{1}{12(1-v^2)}$$

All the dimensional parameters can be written in terms of mass M, time T and length L. It is possible to create $(n-r) = 9-3 = 6$ non dimensional parameters. This set of repeating parameters was chose:

$$[K_s, \rho, D]$$

It is possible to notice that K_s has the dimension of a pressure. It allowed not to divide the pressures for the kinematic pressure, that changes with the Reynolds number. Starting from these repeating parameters, the non dimensional parameters were:

$$\left[\frac{u}{\sqrt{\frac{K_s}{\rho}}}, \frac{u}{D\sqrt{\frac{K_s}{\rho}}}, \frac{p_{12}}{K_s}, \frac{p_{e2}}{K_s}, \frac{L}{D}, \frac{t}{D}\right]$$

According to Buckingham's theorem, once all the non dimensional parameters are matched, the behavior of the system is the same: even if Reynolds number does not appear in the non dimensional parameters, when all the others are the same, the Reynolds is the same. During the experiments, one test where all the non dimensional parameters are almost the same than a literature case was run; this test was used to validate the new system.

Chapter 3

Experimental setup

The experimental setup was similar to the one used in [9], with few modifications (fig 3.1). Two water reservoirs with different fluid height generated the pressure difference to move the flow inside a starling resistor. The collapsible tube with internal diameter D was located in a chamber where the pressure could be changed. The working liquid was water for the preliminary experiments and a mixture of water and glycerin for the final one.

A centrifugal pump was used to move the fluid from a discharge reservoir to the upstream one. The fluid level was kept constant inside the buckets thanks to a sink. The volume of the water reservoirs upstream and downstream was about 4 liters, enough to have very low flow velocity inside the buckets. In the first version of the setup, the pump was directly connected with the upstream tube. The system was less complex, but it had to be changed because of the mutual interaction between the oscillations in the collapsible tube and the pump cycle.

In the final version of the set-up, the flow path was the following one: starting from the discharge reservoir, the working fluid was pumped to the upstream bucket by the pump; while a part of the flow was conveyed to the collapsible tube, the excess of liquid returned to the discharge reservoir thanks to a back flow loop.

The collapsible tube was connected with two rigid pipes that were made up of clear acrylic and were 40 D and 30 D long respectively. Just upstream of the upstream pipe there was a flow conditioner to reduce the turbulence inside the pipe. The collapsible tube, core of the experiment, was clamped directly between the upstream and downstream pipes.
After passing inside the downstream pipe, the flow passes through a soft PVC tube to be collected in the downstream reservoir. The liquid level of the downstream reservoir was constant and the overflow was sent directly to the discharge reservoir.
The pressurized chamber was filled with the working fluid (water or mixture of water and glycerin) for these reasons: firstly, to avoid to the collapsible tube to sag because of the liquid weight, secondly, because it is easier to create a leak proof chamber for liquids than for gases; thirdly, not to have an effect of the hydrostatic gradient inside the tube. The pressure chamber was not completely filled with the working fluid, in fact without any compressible fluid the oscillations can not appear. The pressurizing air was extracted by a compressor present in the lab.

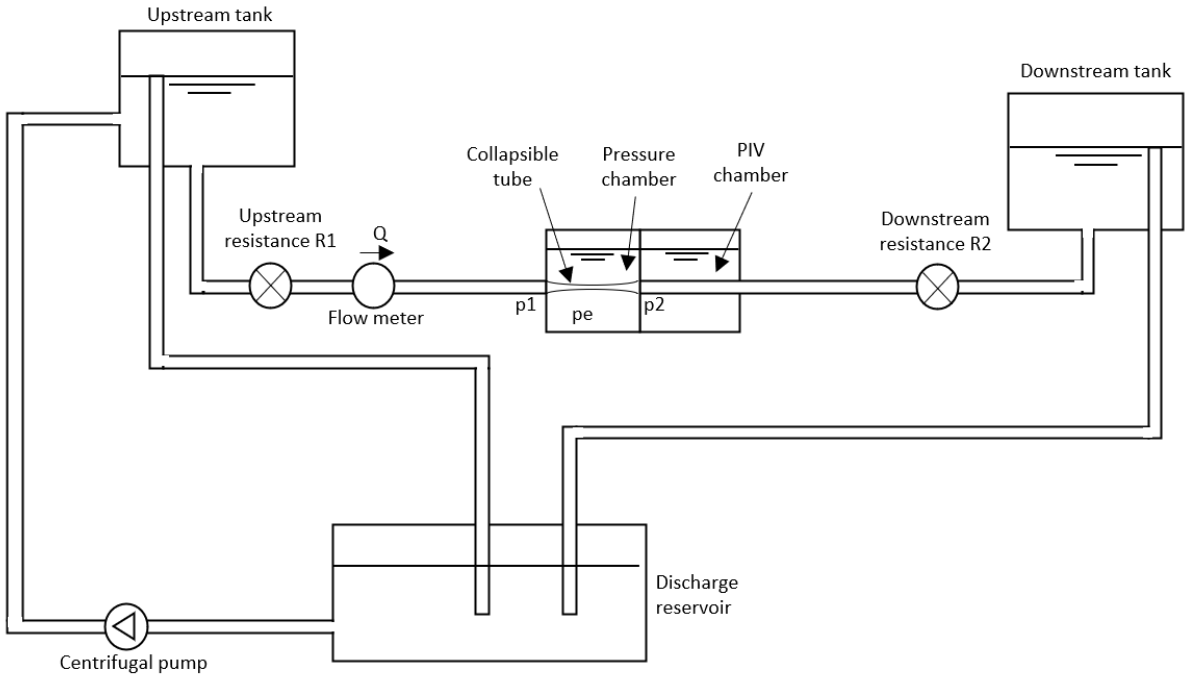

Figure 3.1: Schematic diagram of the experimental set-up

Two solutions were implemented to keep the pressure as constant as possible: the first one is the application of a precise pressure regulator at the exit of the compressor; the second is the use of a 5 gallons reservoir tank that allowed to have a volume of air much higher than the volume oscillations due to the collapse of the tube. The flow rate could be changed thanks to flow valves that were both upstream and downstream of the collapsible tube.

According to [12], the most important parts to be investigated during the self excited oscillations are the tube itself and the downstream pipe. In particular, for this project it was decided to study the collapsible tube applying the Stereo Motion Tracking technique to the tube itself, and the Particle Image Velocimetry to the portion of the pipe just downstream of the tube. An acrylic box divided into two sections was built: the first one was the was the pressurized chamber containing the collapsible tube, clamped between the rigid pipes; the second chamber was open (no lid was required) and partially filled with the working fluid. PIV was performed in the second chamber. The cameras for the Stereo Motion Tracking and for the PIV were located as shown in figure 3.8.
It is useful to call x the axis of the pipe and z the vertical. A laser sheet was created in the "x-y" plane by a laser arm and the PIV cameras were placed perpendicularly.

A 8020 aluminium structure was created to support an acrylic sheet 1" thick, which function was to avoid to the laser sheet to directly hit the free surface of the water, that could be not perfectly calm during the oscillations of the tube.

The pressures just before the collapsible tube (p_1) and just after the collapsible tube (p_2) were measured by Validyne DP15 pressure transducers (accuracy= 0.2kPa), that were calibrated using Delta-Cal 650-950 pressure transducer tester (accuracy=0.13 kPa)
The pressure of the pressurized chamber was measured by a ReliOn 100-021 REL manual

blood pressure monitor that was modified for the experiment.
The flow rate Q was measured by OEM Ultrasonic Flow Measuring System SonoTT™ DIGIFLOW-EXT1 20 cm before the entrance of the upstream pipe; care was taken to ensure at least 15 cm of straight tube before and after the flow meter.
In total two pairs of cameras were used:

- 2 Phantom VEO 440 cameras for Stereo Motion Tracking
- 1 Phantom VEO 4K 990L camera for PIV to have higher-quality data

The laser that used for PIV was Photonics Industries DM30-507DH.

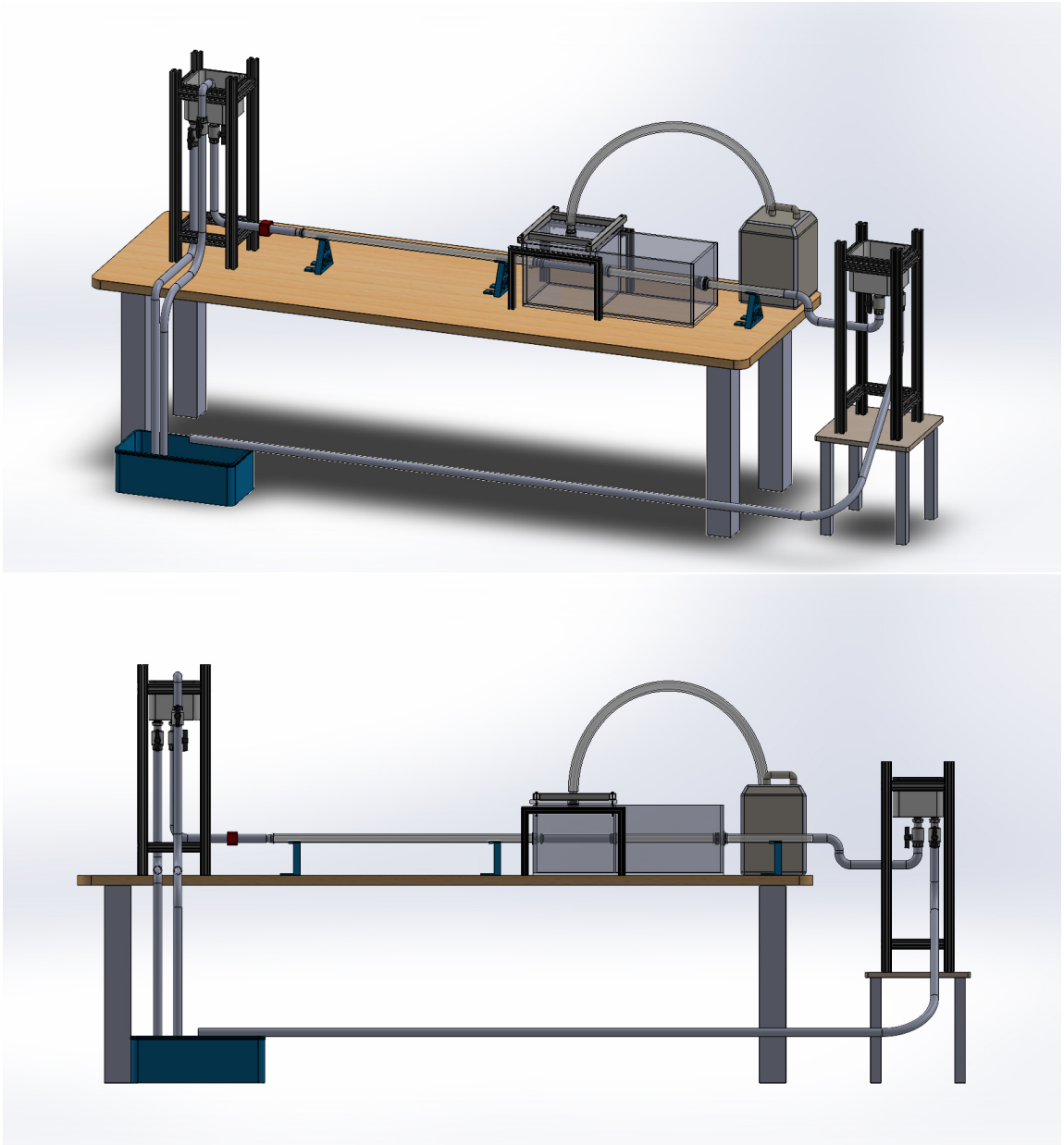

Figure 3.3: 3D views of the experimental set-up

3.1 Collapsible Tube Construction

The Collapsible tube is the most important part of the experimental setup, and its properties strongly influence the behavior of the flow.
Thanks to the non-dimensional analysis of the problem, the parameters that determine the properties of the problem are defined.
In particular, the following non-dimensional quantities are related to the tube itself:

1. L/D_i the ratio between the length of the collapsible tube and its internal radius. To determine this quantity, a compromise has to be found between a long collapsible tube (that can lead to sagging of the tube) and a short one (where the behavior is dominated by the tube tension) [9]

2. t/D_i: ratio between the thickness of the tube and its internal diameter. Increasing this ratio, the stiffness of the tube increases. It is possible to notice that this parameter appears twice in the non-dimensional analysis: once alone and once in the K_s parameter, where there is its third power.

3. K_s: Stiffness parameter. This parameter is often used in structural problems and it is related to the Young modulus of the material, to the Poisson number, and to the t/D_i ratio.

The dimensions of the collapsible tube were chosen to be in line with the previous experimental works. In Table 3.1, a review of the dimensions found in the literature is presented. In the first row, it is possible to find the Reference. It is important to notice that some of the cited articles do not report all the dimensions of the collapsible tube.

		[7]	[9]	[1]	[5]
D: internal diameter	mm	10	12.7	12	13
L: lenght	mm	147	120	228	213
t: thickness	mm	0.7	0.33	1	/
E: Young's modulus	MPa	0.56	1	/	/
L/D	/	14.7	9.45	19	16.4
t/D	/	0.07	0.026	0.08	/

Table 3.1: Dimensions of collapsible tubes found in literature

The dimensions 3.2 have been decided matching the non dimensional parameters L/D_i and t/D_i found in literature. The value of the internal diameter is about the double of the ones that have been previously used. This choice has been taken in order to acquire better data with PIV and SMT.

The tube was created pouring the silicone between an internal circular rod and a concentric external pipe. The pipe was cut in the half, in order to be removed after the curing of the silicone.
The internal rod and the external cylinder were kept aligned thanks to two molds. The molds were made up of three different parts each: two symmetric stamp that could be stuck together and one internal stamp that had a pin to be inserted into the rod.

The molds were 3D printed using Markforged 3D printers. While the top mold (the blue one in figure 3.4) had a squared shape and four walls in the top to collect a little quantity of silicone (not to fill it continuously), the bottom part (black one) had a rounded shape. The reason of this choice is that, during the curing of the silicone, the bottom part was covered by a balloon to avoid leaks (see fig. 3.4, right image).

Other strategies that have been applied in order to minimize the silicone leaks during the curing included applying a layer of tape along the external cylinder and a layer of dental glue (waterproof and very rapid curing time) in the upper mold. The silicone cured for at least 24 hours. Curing time can be reduced if silicone is kept at high temperature, but the 3D printing molds were sensitive to heat and would have bent. Increasing the curing temperature, Young's modulus increases.
Tattoo paper was used to cover the external surface of the collapsible tube (figure 3.5) in order to improve the quality of the Stereo Motion Tracking results.

L/D	t/D	E	D	t	L
10	0.074	1.55 Mpa	2.54 cm	2 mm	25.4 cm

Table 3.2: Collapsible tube dimensions

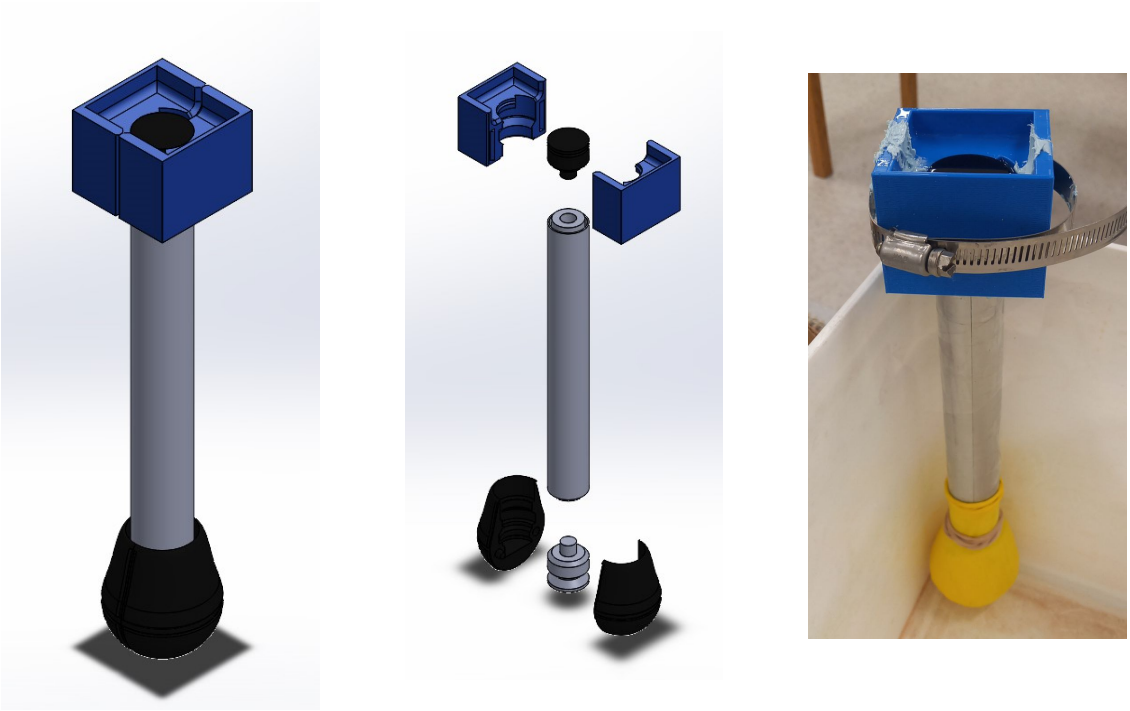

Figure 3.4: Collapsible tube construction method: 3D view of the assembly (left), exploded view (center) and figure of the real assembly with the yellow balloon in the bottom part (right)

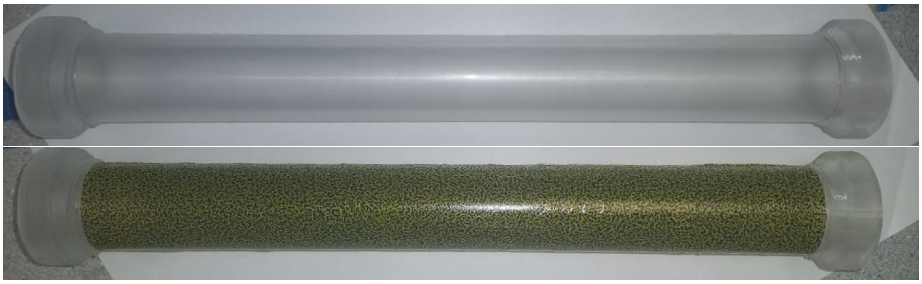

Figure 3.5: Collapsible tube before (top) and after (down) the application of the tatoo paper

3.2 Collapsible tube Young's modulus

The mechanical properties of the collapsible tube are represented by the K_s parameter, which is a function of t/D_i and the Young's modulus. The first is a geometric parameter that is easy to determine, while the latter has to be determined from a Dynamic Mechanical Analysis (DMA). During the manufacturing of the collapsible tube, a part of the silicone was placed in a rectangular mold, which was later used to determine its elasticity modulus. For the computation of the Young's modulus, a DMA test was carried out. During the test, one end of the specimen was fixed, and the other one was clamped to a mechanism that could move. Starting from the values of the applied force and the elongation of the specimen, it was possible to plot a stress-strain diagram.

$$\sigma = \frac{F}{A} \tag{3.1}$$

$$\epsilon = \frac{l - l_0}{l_0} \tag{3.2}$$

Young's modulus was computed as the derivative $E = \frac{d\sigma}{d\epsilon}$, considering the region where $\epsilon < 0.1$ (red rectangle in figure 3.6) because the strain of the collapsible tube during oscillations is usually less than 5 %.

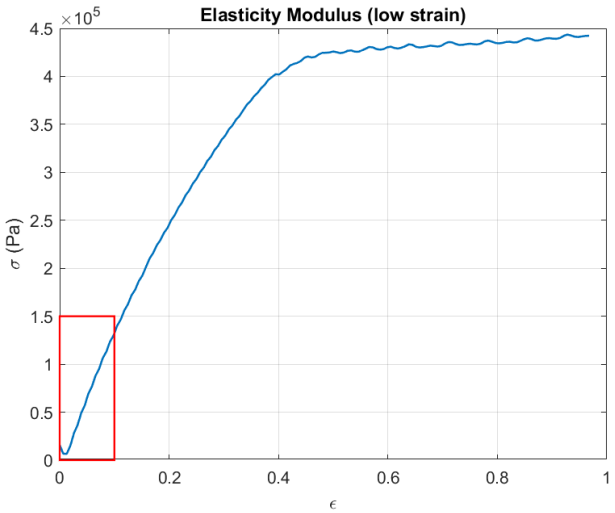

Figure 3.6: Stress strain diagram for Sylgard 184 with ratio 5:1. The Young's modulus has been computed considering $\epsilon < 0.1$

Image 3.6 shows the stress-strain diagram for the silicone used in the definitive experiment, where the value of Young's modulus was E=1.55 MPa. It is possible to notice that until $\epsilon = 0.4$, stress and strain are linearly dependent.

For the experiments, Sylgard 184 (with a high Young's modulus) and Ecoflex 00-30 by Smooth-on were used. According to the literature, it is possible to mix these silicons to obtain intermediate values of the elasticity modulus. For this reason, a set of tests was carried out by changing the ratio of the mixture to match the desired Young's modulus (tab. 3.3).

Name	Sylgard 184	Ecoflex 00-30	Sylgard : Ecoflex ratio	E [MPa]
Sylgard 5:1	5:1	\	\	1.55
Syl_Eco_1_1	10:1	1:1	1:1	0.398
Syl_Eco_3_1	10:1	1:1	3:1	0.511
Syl_Eco_5_1	10:1	1:1	5:1	0.554

Table 3.3: Young modulus of different mixture

3.3 Flow conditioner

Every flow, after entering in a pipe, needs a certain axial distance form the entrance before being frozen, i.e. having a situation where $u = u(r)$. This distance is named entry length L_e, that is a function of the Reynolds, of the type of flow and of the internal diameter of the pipe D_i. In particular, experimental results proved that for laminar flow and for turbulent flow it is respectively:

$$L_e = 0.06 \cdot Re \cdot D_i \tag{3.3}$$

$$L_e = 4.4 \cdot Re^{1/6} \cdot D_i \tag{3.4}$$

The entry length is necessary to restore a frozen flow every time that the flow is perturbed for example because of an elbow of the pipe or because of the presence of a flow valve.
The Reynolds numbers of the experiments were initially supposed to be between Re=100 and Re=3000, to reproduce the experiments studied in [12] ; considering the most conservative case, equation 3.3 shows the necessity to have an upstream rigid pipe long at least $L_e = 180 \cdot D_i = 4.57m$. Such a long pipe would be a limitation and would not fit in the laboratory. For this reason it was decided to add a flow conditioner.

The flow conditioner consists of a perforated plate with circular holes; the holes dimension is not constant but decreases with the distance from the axis of the tube. The flow conditioner allows to straighten the flow and it reduces the entry length. Flow conditioners are commonly used in gas pipelines where, to measure the flow rate, a small portion of the flow is sent in a small diameter pipe where a flow meter is present and then sent back again to the main pipe.
The Reynolds's number of these application is high (the order of magnitude is $Re = 10^4 \div 10^5$) and the flow is turbulent; this explains why the most of the experiments that have been carried out in the past (for example [6],[10]) considered turbulent flows. Nevertheless, it was shown that the flow conditioner has a positive effect also in laminar flows [11].

For this reason, a HDPE (High Density Polyethylene) Zanker flow conditioner was manufactured in line with the dimensions provided by [10]. The flow straightener was placed just before the upstream rigid pipe.
The length of the upstream pipe was $40D_i$, enough to ensure fully developed flow until $Re = 650$. Thanks to the use of the flow conditioner, all of the experiments were able to achieve fully developed flow.

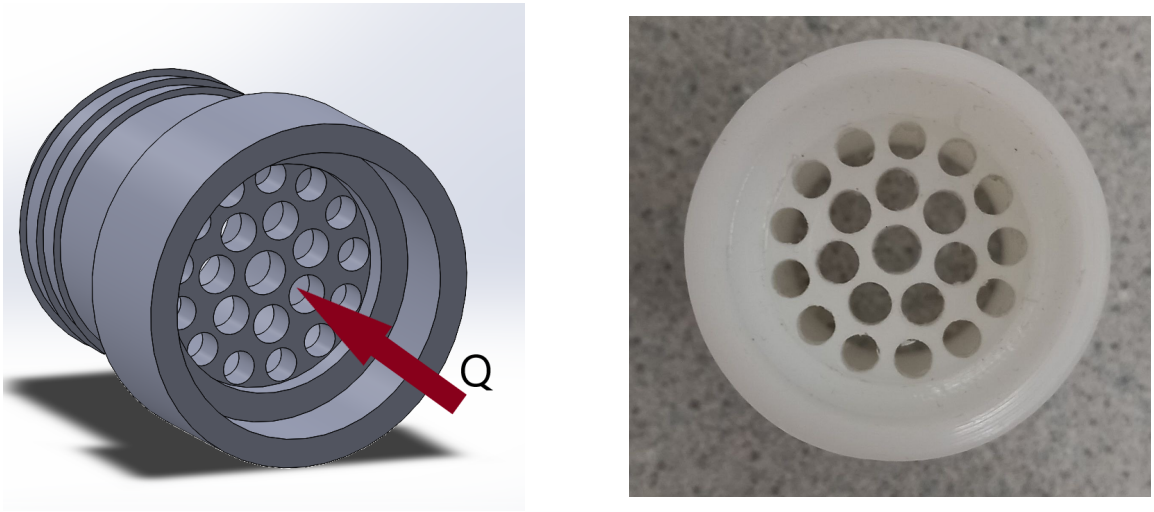

Figure 3.7: Flow conditioner CAD (left) and the model used in the experiments (right)

3.4 Stereo Motion Tracking

The main component of the entire setup is collapsible tube, and its shape has been studied using the Stereo Motion Tracking technique. The tube, clamped between the rigid pipes in the pressurized chamber, was observed by two cameras. The cameras were outside the chamber, at the same height of the collapsible tube and their angular distance was about 10° (fig. 3.8).
Cameras were controlled by PCC (Phantom Camera Control Application) software. To ensure that the figures and the data acquired by the DAQ were synchronized, a trigger (digital signal) was sent from the DAQ to the camera with a coaxial cable.

Starting from the pictures of the camera, a Matlab code was written to use the stereo parameters obtained from the calibration in order to create a disparity map; the map was then converted into a PointCloud, defined as a group of point with known 3D coordinates. The PointCloud was manipulated, removing the noise and focusing only in tube region (deleting all the spurious points). The code operated following these steps:

1. Consider a pair of images (fig. 3.9a, 3.9b)
2. Built a disparity map starting from the figures (fig. 3.9c)
3. Convert the disparity map into a PointCloid (fig. 3.9d)
4. Filter all the points that did not belong to the tube (fig. 3.9e)

5. Find the axis of the uncollapsed tube
6. Rotate the coordinate system in such a way that the axis of the tube was aligned with [1 0 0] vector (fig. 3.9f)
7. Apply this rotation to all the images
8. Edit a video starting from the couples of images

It was in fact important to have a horizontal axis of the tube, to be able to insert in the same plot both the Stereo Motion Tracking data and the PIV ones.

3.5 Particle Image Velocimetry

Particle Image Velocimetry (PIV) is an optical technique that allows to determine the velocity of flow.
Usually the flow is seeded with some particles that follow it; the flow is illuminated by a laser sheet that creates a plane. An high speed camera (or more for more complex versions) is perpendicular to the laser sheet and detects the position of the seeding particles.
PIV seeding particles are highly refractive or fluorescent; for this reason, the camera detects peaks of light intensity and determines the position of the particles in the field of view.
Starting from a couple of images acquired with a time difference Δt, it is possible to compute the velocity of each particle if it is known the location in both images using:

$$\bar{v} = \frac{\bar{\Delta} x}{\Delta t} \tag{3.5}$$

Unfortunately, it is impossible to track every single particle (for examples if the particles have a component orthogonal to the laser sheet can disappear) and an alternative method is implemented: the entire field of view is divided into squared smaller regions (usually 64x64 Pixels or 32x32 Pixels), called interrogation regions. The size of these regions has to be big enough to contain a representative amount of seeding particles.
After tracking the location of the particles (that can be determined with sub-pixel accuracy), it is possible to find the maximum of cross-correlation function for each interrogation region:

$$R(r,s) = \sum_{i=0}^{D_I/2} \sum_{j=0}^{D_I/2} IA_1(i,j) IA_2(i+r, j+s) \tag{3.6}$$

where D_I is the size (in pixels) of the first square interrogation region, IA_1 and IA_2 are the intensity values from the first and second image and r, s are x and y component of the displacement of the interrogation window. The maximum of the cross-correlation function indicates the more probable displacement of the particles. Even if there are many different types of PIV, it was used the simplest one in this thesis: 2D-2C (two dimension two component) PIV allows to have a knowledge of the velocity field in the laser sheet plane. Using this method implies that the velocity component perpendicular to the laser plane is neglected.

Phantom VEO 4K 990L camera was used to acquire the images and the laser source was

Photonics Industries DM30-507DH. This laser is dual head, that means that two laser pulses can be created in a very short time interval.The images were acquired using the Frame-Straddling Mode.

Necessary for the PIV are the seeding particles, that must have peculiar properties: they have to be big enough to be detected by the cameras but small enough to have very low mass to follow the flow. They also must have a density similar to the working fluid's one (to avoid buoyancy forces). For the experiments PMMA rhodamine fluorescent particle with 63-75 μm mean diameter were used.

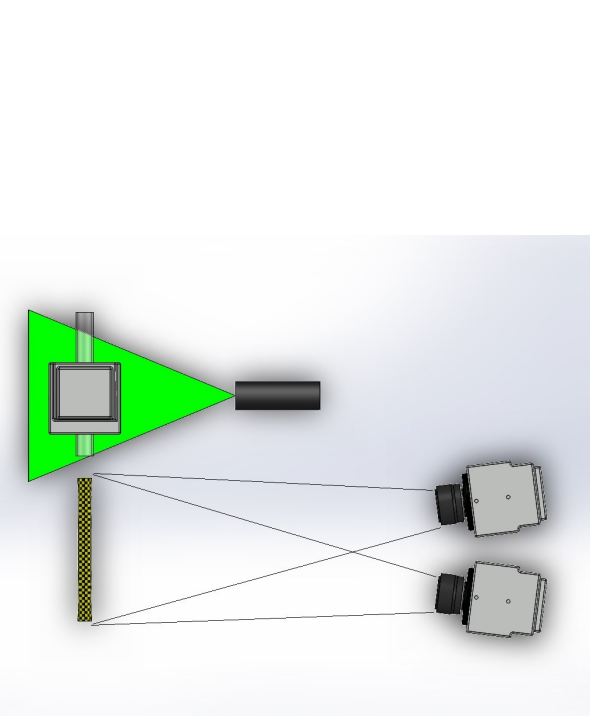

(a) x-y plane

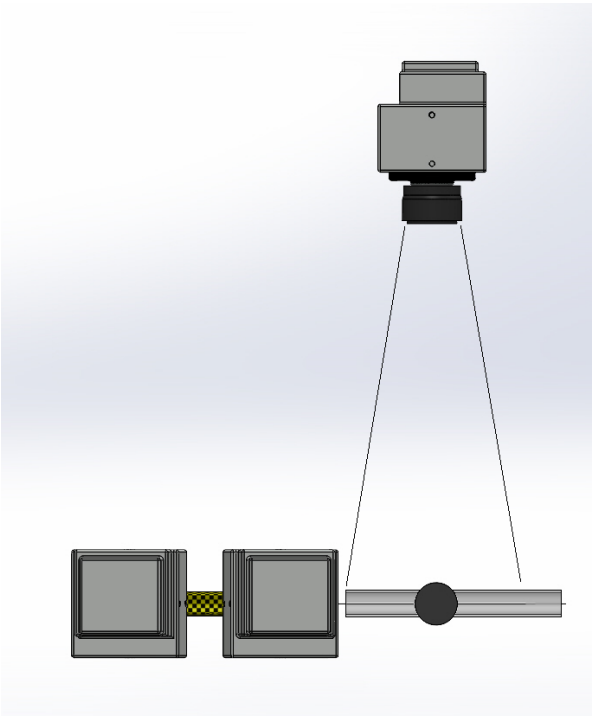

(b) x-z plane

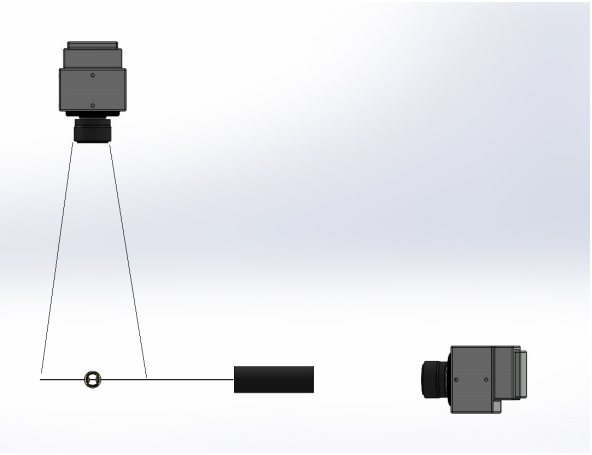

(c) y-z plane

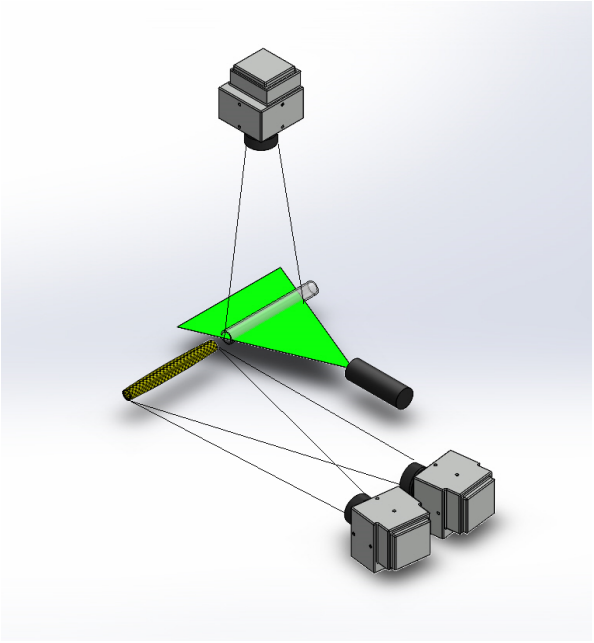

(d) 3D view

Figure 3.8: Simplified CAD of the position of the cameras. Stereo Motion Tracking cameras are watching the x-z plane and the PIV's one is taking images of the x-y one.

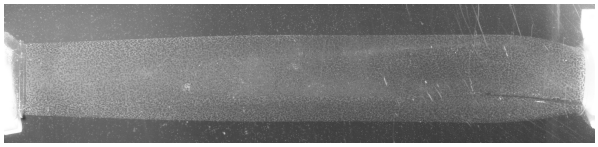

(a) Left camera

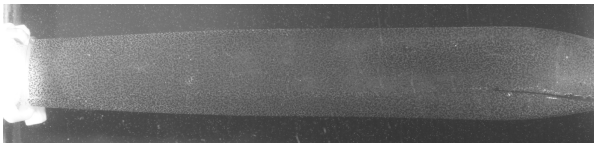

(b) Right camera

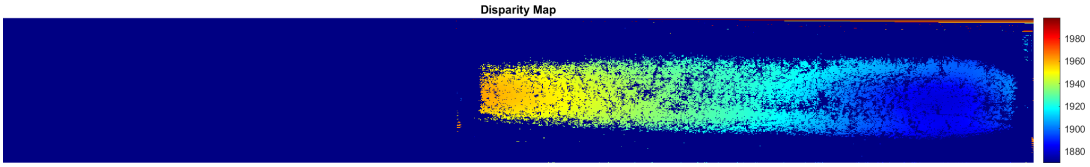

(c) Disparity Map

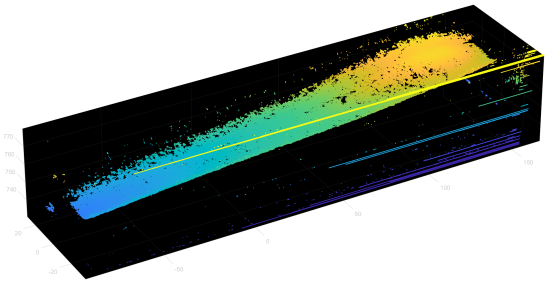

(d) Initial Pointcloud

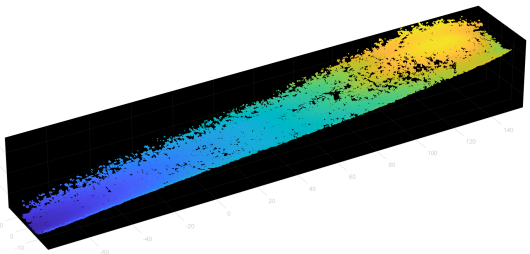

(e) Filtered Pointcloud

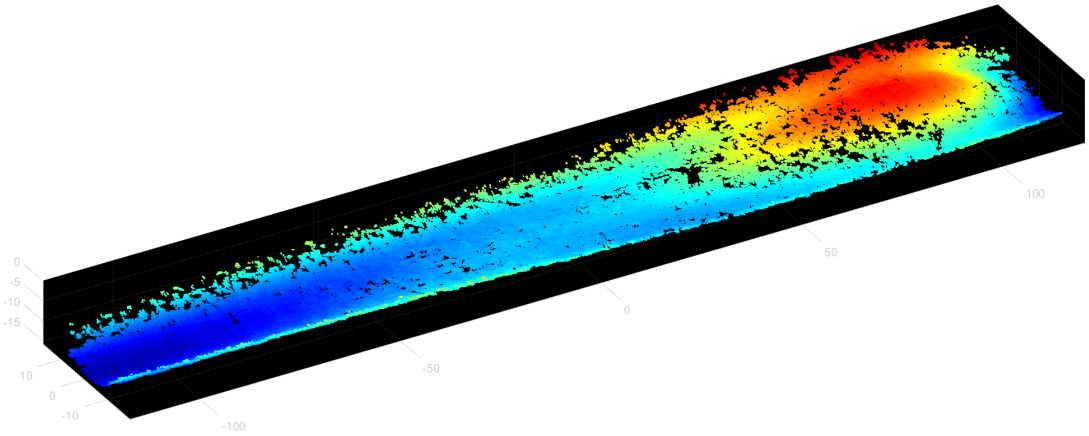

(f) Filtered and rotated Pointcloud

Figure 3.9: Stereo Motion Tracking procedure

Chapter 4

Methods

The experimental setup allowed to acquire a big amount of data at the same time. Due to its complexity, it was decided not to implement the final version of the setup suddenly but to gradually increase the complexity of the experiments.

This is the sequence of experiments that were carried out:

1. Test with Flow meter and pressure transducers (working fluid: water)
2. Test with Flow meter, pressure transducers and Stereo Motion Tracking (working fluid: water)
3. Test with Flow meter, pressure transducers and Particle Image Velocimentry (working fluid: water)
4. Test with Flow meter, pressure transducers and Stereo Motion Tracking, Particle Image Velocimetry (working fluid: water)
5. Test with Flow meter, pressure transducers and Stereo Motion Tracking, Particle Image Velocimetry (working fluid: glycerin)

In the following sections only the test number 5 will be described because it is the most complex experiment and includes all the methods of the previous ones.

4.1 Calibrations

4.1.1 Flow Meter Calibration

The first phase of the method was the calibration of the flow meter and of the pressure transducers. To calibrate the flow meter a simple flow circuit was created, made up of a water reservoir, a pump, a resistance and a graduated bucket. After turning on the pump, the resistance was kept constant (as well as the flow rate) and the water was collected in the graduated bucket.
Once known the volume of the water collected and the elapsed time, it was easily computed the volumetric flow rate inside the channel as:

$$Q = \frac{V}{\Delta t} \tag{4.1}$$

The output of the flowmeter was a voltage value that was read by a LabVIEW code. It was then computed the average value of tension and a Flow rate - Voltage diagram (fig. 4.1) was created.

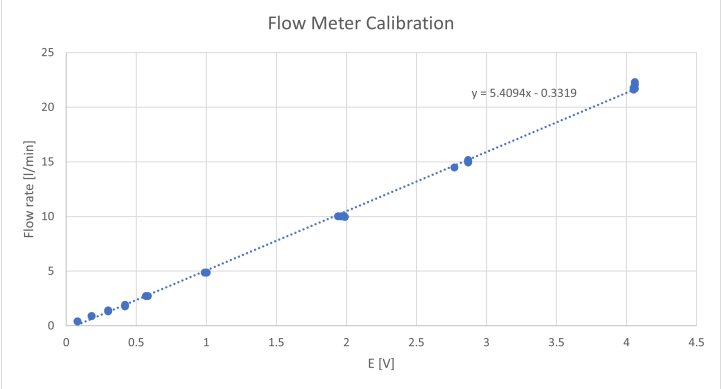

Figure 4.1: Calibration Diagram for the flow meter

After noticing that the correlation between the two dimensions was linear, the calibration constants were computed applying the last squares method.

4.1.2 Pressure transducer calibration

A similar procedure was used to calibrate the pressure transducers. A pressure transducer calibrator was connected through a pneumatic line to the pressure transducer. The calibrator had a handle that was possible to round in order to change the pressure inside the pneumatic line.

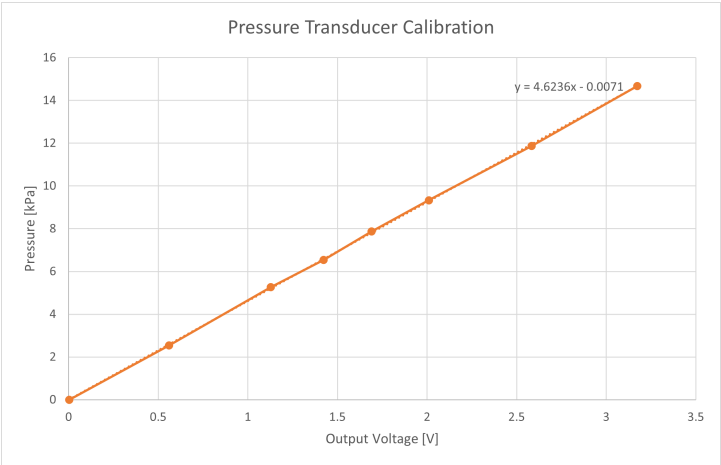

Figure 4.2: Calibration Diagram for the pressure transducer

The pressure was displayed on the monitor of the pressure calibrator, and at the same time the analog signal from the pressure transducer was sampled using the CDaq and the mean of the signal was computed thanks to a LabVIEW code.
As in the previous case, the data were plotted in a pressure - voltage diagram in order to obtain the calibration constants of the pressure transducer (fig. 4.2). Also in this case, the function was linear.

4.2 Setup preparation

In the second phase of the preparation the working fluid was added to the setup. A mixture of water and glycerin (30:70 w:w), bought from Chemworld.com, was poured directly in the backup reservoir and pumped all over the system; the fluid was also added in the PIV chamber (until it reached the acrylic sheet) and in the pressurized chamber (at that moment it was open). The fluid level inside the pressurized chamber was the same for all the tests, not to change boundary conditions from experiment to experiment.

In this phase the collapsible tube was mounted between the rigid supports in the pressurized chamber (during PIV and Stereo Motion Tracking calibration it will be removed). Flow valves were opened to have a flow inside the pipe, the pressure transducers were connected to the pressure taps upstream and downstream of the collapsible tube and the flow meter (previously calibrated) was mounted. The LabVIEW code was run to check that pressures and flow rate data were acquired as expected. Later, all the flow valves were closed, the pump turned off and the collapsible tube removed to start the calibration of SMT and PIV.

4.2.1 Stereo Motion Tracking Calibration

Before the actual recording, the calibration of the cameras was done using Matlab Stereo Camera Calibration Toolbox. During the calibration phase, the collapsible tube was removed and a checkerboard plate was moved inside camera's field of view (see fig. 4.3). Stereo Camera Calibration Toolbox detected the corners and required the dimension of a single square as input. This Toolbox keeps into account the different refractive indexes air-acrylic and acrylic-operating fluid. The output of the Stereo Motion Calibration are the Stereo parameters (necessary to compute the disparity map of the collapsible tube and the 3D coordinates of the collapsible tube).

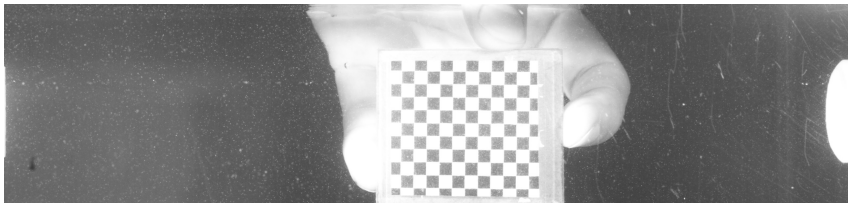

(a) Camera's image of the calibration plate

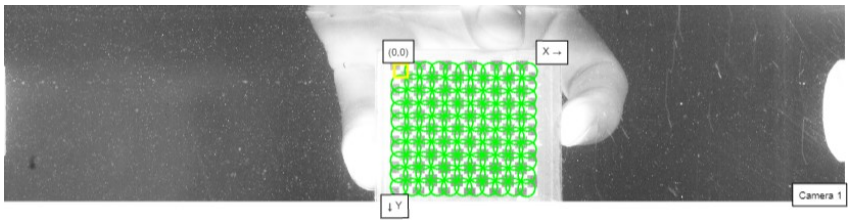

(b) Detection of origin (yellow) and corners (green) using Stereo Camera Calibrator toolbox

Figure 4.3: Stereo Camera calibration

4.2.2 PIV calibration

Particle Image Velocimetry (PIV) was conducted using the LaVision software, a commonly used tool in fluid dynamics research. A significant challenge with this technique is the variation in the refractive index between the working fluid and the acrylic material, with the latter having a higher index of refraction ($n = 1.48$). To address this issue, a mixture of water and glycerin with a lower index of refraction ($n = 1.41$) was utilized instead of pure water ($n = 1.33$).

As shown in Figure (3.8), PIV was performed in the x-y plane. To obtain clear and accurate results, the PIV camera was positioned above the downstream pipe, and special requirements had to be respected to avoid the interference with the free surface of the working fluid. To overcome this challenge, an aluminum structure was designed and constructed to support a transparent acrylic sheet with a thickness of 1.2 cm (fig. 4.4a). This structure effectively eliminated any interference from the free surface of the working fluid and allowed for the collection of high-quality PIV data.

Overall, the use of LaVision software in conjunction with careful experimental design and specialized equipment allowed for successful PIV measurements to be performed, yielding valuable insights into the fluid dynamics of the system under study.

To calibrate the Particle Image Velocimetry (PIV) system, a calibration plate was fabricated using an aluminum rod of identical diameter as the PIV's pipe. Material was subsequently removed from the rod to produce a flat surface with protruding markers in a predetermined pattern (refer to Fig. 4.4b). The separation distance between the markers and their known spacing facilitated the conversion of image pixel dimensions to physical units (i.e., mm). After the PIV calibration, the collapsible tube was mounted again and the pressure chamber was closed with the acrylic lid.

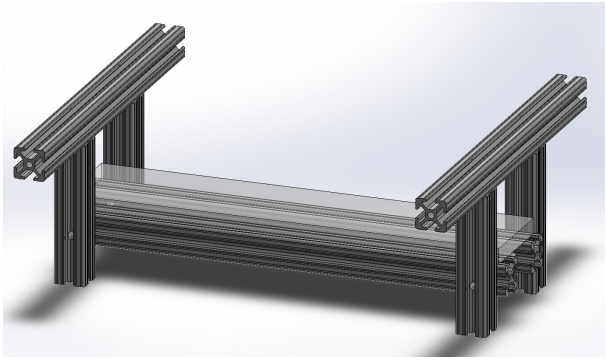

(a) Aluminium 8020 structure

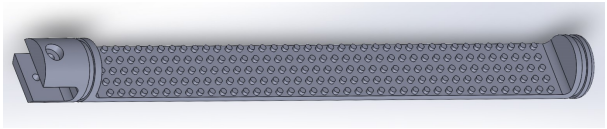

(b) Calibration plate for PIV

Figure 4.4: Solidworks models for PIV

4.2.3 LabVIEW Code

LabVIEW software was utilized to facilitate data acquisition and synchronize the cameras. Specifically, upon executing the LabVIEW code, two analog output signals were transmitted to the Particle Image Velocimetry (PIV) and Stereo Motion Tracking (SMT) cameras, respectively.
This action also initiated the data acquisition process from the flow meter and pressure transducers, situated upstream and downstream of the collapsible tube, respectively. The LabVIEW code then processed the analog input signals from the flow meter and pressure transducers and utilized the previously obtained calibration curves (fig. 4.1 and 4.2) to convert their respective values.

Chapter 5

Results

5.1 Tube Law

The aim of this preliminary experiment that was carried out was to see if the collapsible tube followed (as expected) the tube law. Two different cases were studied: in the first one the flow rate was equal to zero, in the latter it was different. In both the cases the major axis of collapse of the tube was coincident with the x-z plane.

Starting from the first case, it is possible to see (fig. 5.1) that, when the trans-mural pressure was zero (i.e. when the pressure inside and outside of the collapsible tube is the same), the area ratio A/A_0 was one and the shape of the tube is circular (fig. 5.2a). When the external pressure was increased, the trans-mural pressure decreased to negative values and the shape was still almost circular. Until values of $p_{tr} = -1.3$ kPa the area did not have significant changes (purple circle in the figure).
After that point, when the external pressure was slightly increased, the cross-sectional area of the tube decreased and the shape was more elliptic than in the previous points (fig. 5.2c); the dumbbell shape of the tube started be evident.

Then there was a region when the area was very sensitive to the intramural pressure and even very small changes in pressure created big area changes: when p_{tr} passed from -1.3 kPa to -1.8 kPa, the Area ratio passed from 0.96 to 0.24 and the tube had a dumbbell shape (fig. 5.2b).
After that point, the area became almost independent from the external pressure and the shape was similar to a dumbbell (fig. 5.2d).

The second case considered (fig. 5.3) was obtained using water as working fluid; the mean flow rate was $\overline{Q} = 1.2$ l/min that means that the Reynolds number was about $Re = 1000$. As it is possible to see from fig. 5.3, the behavior of the collapsible tube was essentially the same: in the upper region of the map the shape is almost circular and the area similar to the reference one; then there is a step when the area drastically reduces before being almost constant and dumbbell shaped.
Less data were recorded for Re=1000 and unfortunately the partial collapse of the tube was not obtained. For this reason the cross sections of the tube are not presented.

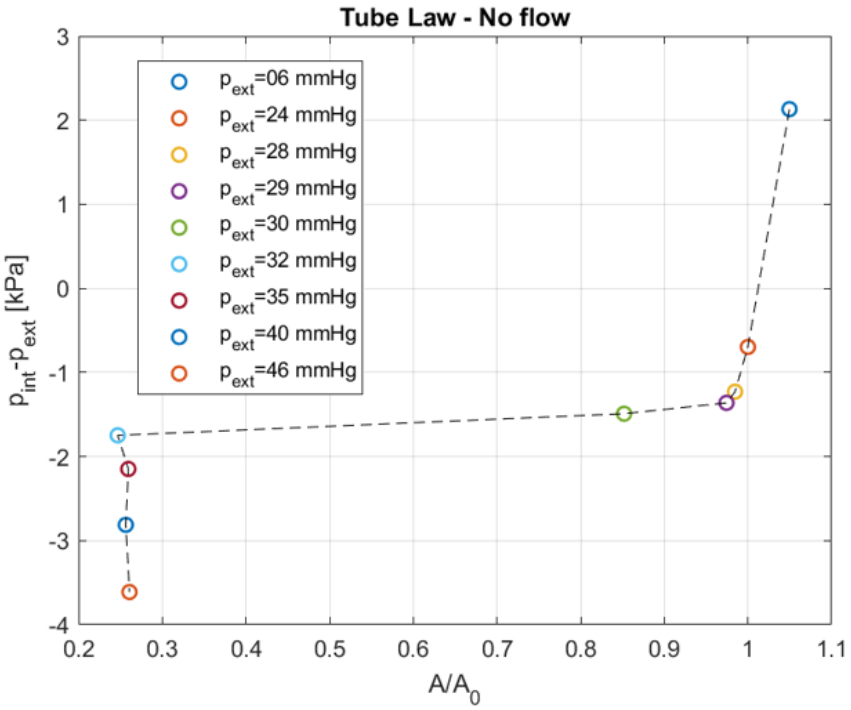

Figure 5.1: Tube law - Zero flow rate case

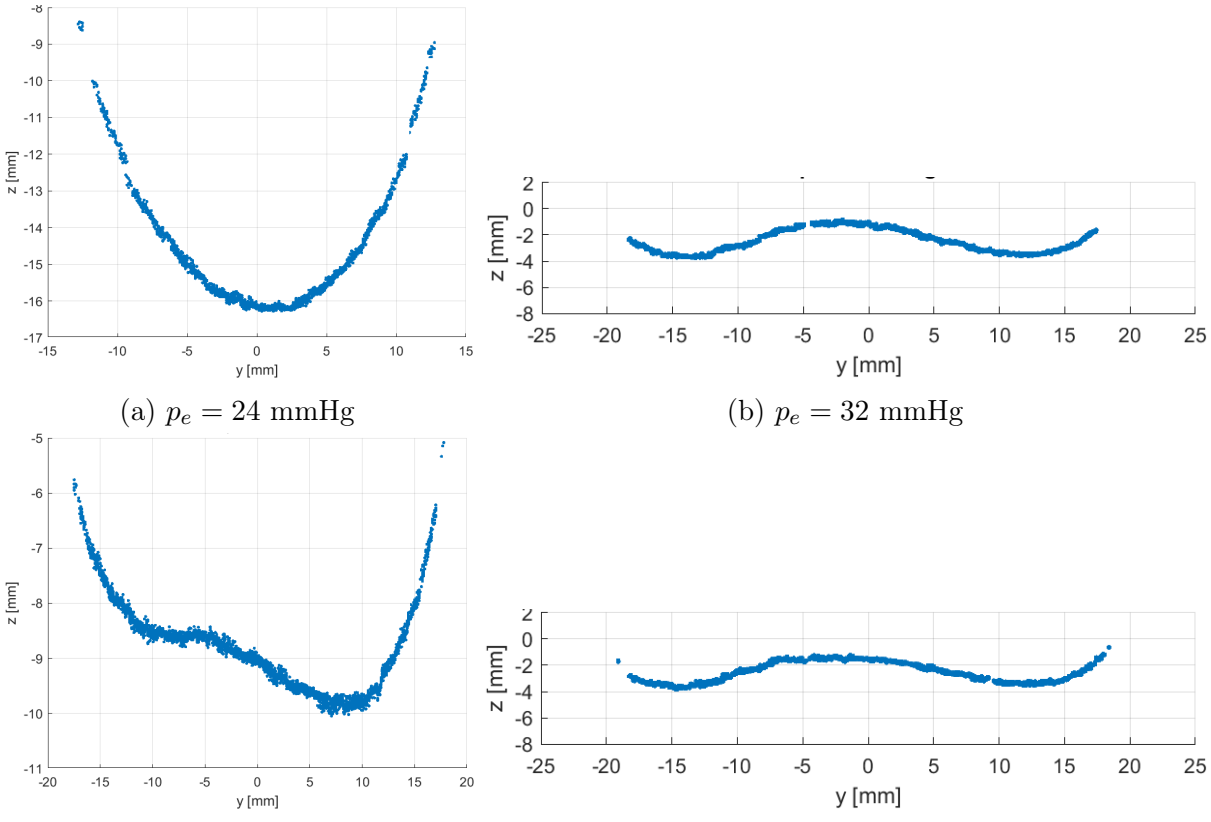

(a) $p_e = 24$ mmHg

(b) $p_e = 32$ mmHg

(c) $p_e = 30$ mmHg

(d) $p_e = 46$ mmHg

Figure 5.2: Cross sectional shape of the tube at different values of external pressure of figure 5.1

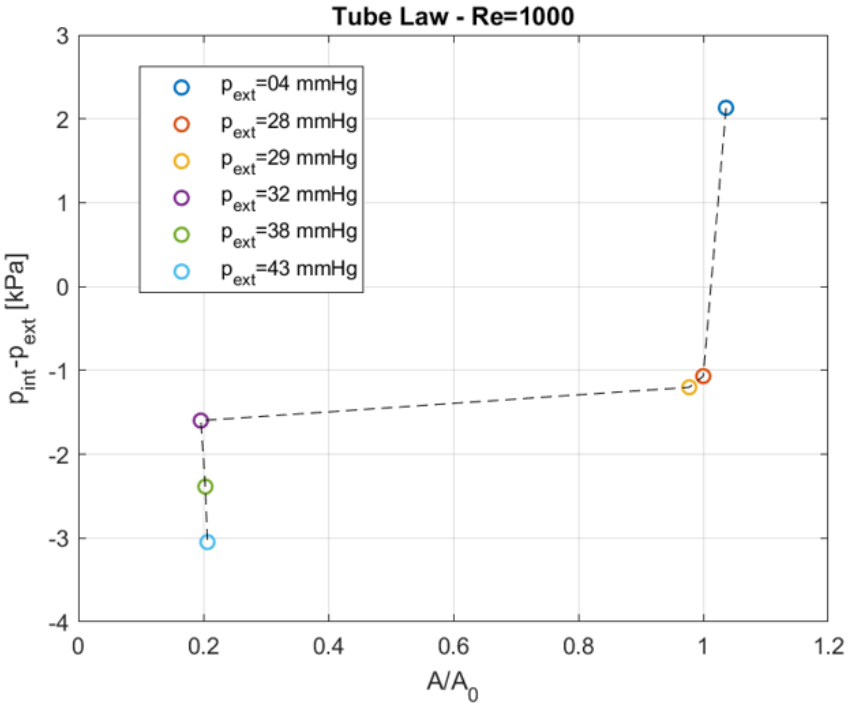

Figure 5.3: Tube law when the Reynolds number is 1000

5.2 Tube characterization

The goals of this preliminary test were to check that the flow meter and the pressure transducer were working correctly and to create a Flow rate - transmural pressure diagram. While the first phase of this experiment was carried out using water as working fluid, the second one used water and glycerin. The fluid level in the upstream reservoir was $H_u = 60$ cm and in the downstream one $H_2 = 20$ cm above the axis of the tube.

The experiment was carried out adjusting the flow rate with the upstream flow valve R1 as first; after, the pressure of the pressurized chamber was gradually increased and every time that the system was experiencing different behavior of the collapsible tube, p_e was recorded. Three different situations were found in this preliminary experiment:

1. Steady case - Tube completely open
2. Oscillating case
3. Steady case - Tube collapsed

After reaching the condition of steady collapse, the external pressure was incremented again to be sure that there were not relevant phenomenon any more. Afterword, the upstream resistance R1 was decreased, and the same procedure was applied again.

In the first image presented (fig.5.4), there are the results obtained in the case with water. In the figure it is possible to see that for low flow rates (and low Reynolds numbers) there were only two cases: when the external pressure p_{cr}, the the tube was completely open and there were no oscillations. This means that all the fluid dynamics properties were almost constant (flow rate, pressure, shape of the tube).
When the external pressure reached p_{cr}, the tube started to collapse. The collapse of the tube happened gradually: usually between the start and the end of the process the external pressure increased by 2-3 mmHg. In these cases the properties were steady as well.
When the external pressure was increases, the tube completely collapsed; in the following sections will be seen that the pressure drop through the ends of the tube increases (higher resistance) and that the flow rate diminishes (because the flow is choked). Again, the fluid dynamics properties were almost constant in this case.

When the flow rate was high enough to have a $Re > Re_{cr}$, the possibilities were three:

- when p_e is lower that the pressure inside the tube the tube is open and the case is steady
- for intermediate p_e, the tube starts to oscillate. During the oscillations, both the fluid dynamic properties and the shape of the tube are changing periodically.
- for high p_e, the tube is completely collapsed and the case is steady

In the figure 5.4 it is possible to notice that for the case with only water the flow rates at which the oscillations occurred were high. It determines that the Reynolds number is very high as well. For example, in the case considered the oscillations appear at:

$$Q_{cr} = 15.97\,\mathrm{L\,min^{-1}}$$

$$Re_{cr} = \frac{4 \cdot \cdot Q_{cr}}{D \cdot v \cdot \pi} = 13169$$

When only water is used, the flow rate does not change significantly from the open to the collapsed configuration, as long as there are no oscillations. However, in the presence of oscillations, the flow rate decreases more significantly (case on the right of the figures).

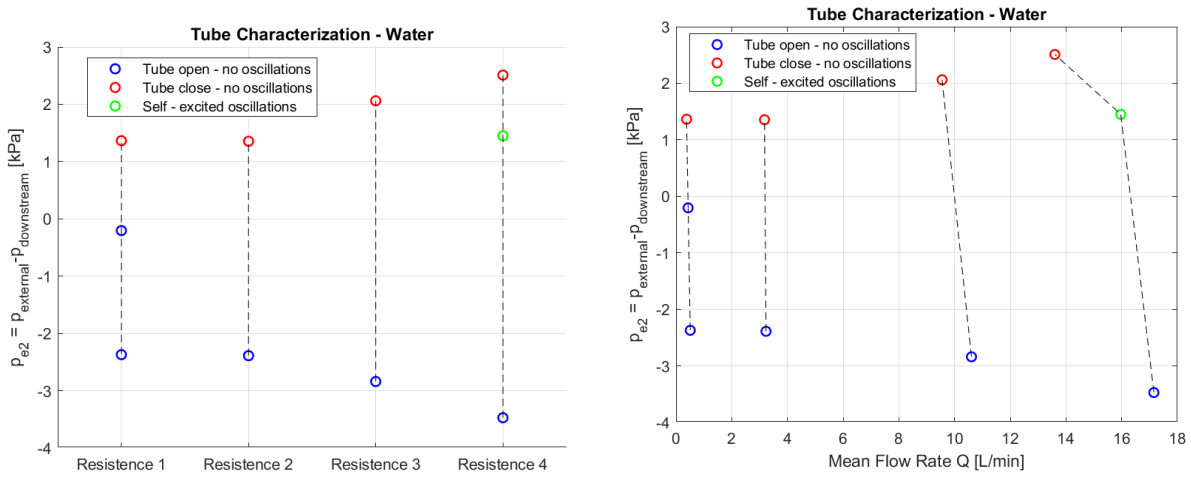

Figure 5.4: Tube characterization in the case with only water

The only difference between the left and right graphs presented in figures 5.4 and 5.5 is the x-axis: the left graphs have the resistance values and make easier to understand the method that has been used to obtain the data (fixing the upstream resistance and changing the external pressure), while the right ones have the mean flow rate. In all the graphs, the data collected with the same upstream resistance are connected through a dotted line.

When the working fluid is 70:30 glycerin:water mixture (fig. 5.5) the critical flow rate was lower than in the previous case and the viscosity of the fluid was higher. For this reason there was a strong reduction of the Reynolds number compared to the case with only water; in fact, considering that the critical flow rate:

$$Q_{cr} = 8.74\,\mathrm{L\,min^{-1}}$$

$$Re_{cr} = \frac{4 \cdot \cdot Q_{cr}}{D \cdot v \cdot \pi} = 430$$

Another notable observation is that, while the value of p_{e2} during the transition from an open tube to oscillations is nearly identical for all three resistances considered, the value of p_{e2} during the transition from oscillations to tube collapse increases with the flow rate (or decreases with resistance).

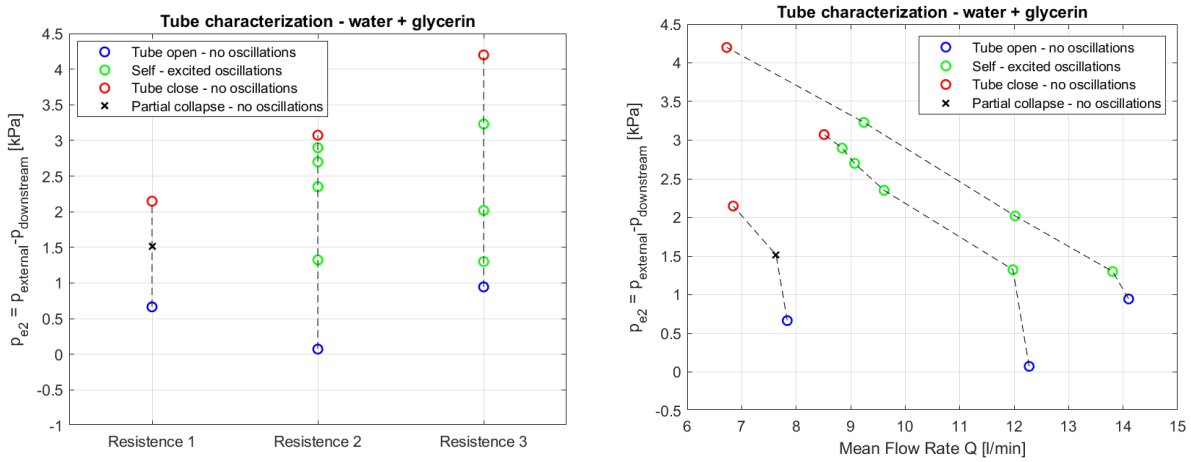

Figure 5.5: Tube characterization in the case with water and glycerin

5.3 PIV validation

The case considered is the one studied in section 5.4.1, where the Reynolds number was $Re = 574$, the tube was completely open and the flow was steady. Because of the low Reynolds number, the flow inside the pipe was laminar. In figure 5.6 it is possible to see the flow field inside the pipe obtained thanks to the PIV. Instead of using a single velocity field, a time averaged one has been considered. 144 frames have been considered (acquisition frequency=24Hz, acquisition time=6s).
During this experiment the flow field computed from PIV was very steady and considering the time average or a single frame would not change the results. For better representation, only one vector each 10 in the x direction was shown in the figure. It is possible to see that the flow field was almost independent from the x direction (frozen flow) and it is clearly visible the parabolic profile of the velocity. The y component of the velocity was negligible everywhere.

In figure 5.7 a comparison between the Poiseuille flow field and the one just downstream of the collapsible tube is presented. The velocity profile plotted is both time averaged and space averaged along the x-axis:

$$u_x(y) = \frac{1}{\Delta t \cdot \Delta x} \int_{x_{max}}^{x_{min}} \int_0^t u_x(x, y, t)\, dt\, dx \tag{5.1}$$

In the figure it is possible to see that the profile obtained is parabolic and it is very close to the one obtained with the Poiseuille equation. Everywhere the velocities are almost coincident with the theoretical previsions; this confirms the good quality of the data acquisition.

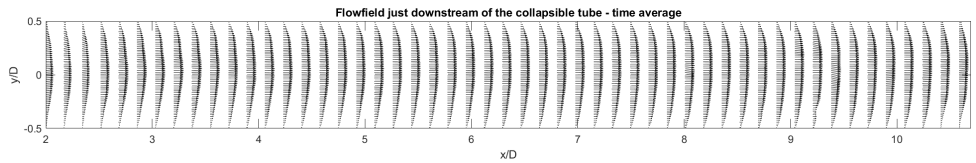

Figure 5.6: flow field just downstream of the collapsible tube in the case 1.1.

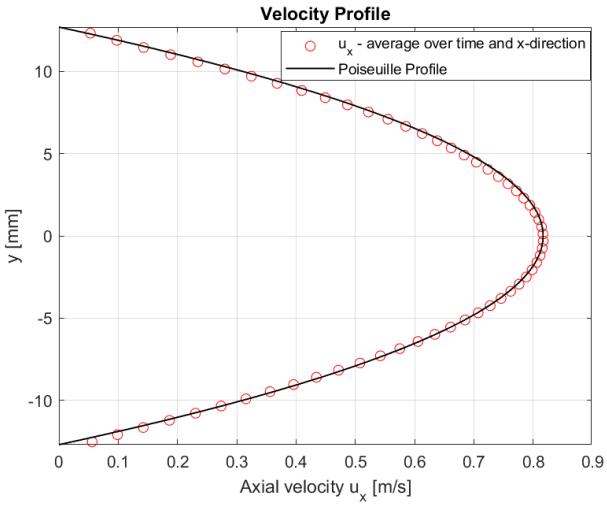

Figure 5.7: Velocity profile inside the downstream pipe compared to the theoretical one obtained from the Poiseuille equation

5.4 Final experiment

The final experiment was run using the water and glycerin mixture as working fluid and a silicone with E=1.55 MPa. The following data were obtained: p_1, p_2, p_e, Q, the shape of the tube and the flow field just downstream of the collapsible tube. The initial idea was to run experiments inspired to the CFD article [12], where they studied the influence of some non dimensional parameters keeping constant all the other one. In this study two main cases were studied:

1. $p_{upstream} = const$ **experiments**
   This first set of experiments was carried out keeping constant the upstream resistance R1 and increasing the external pressure p_2. This leaded to an almost constant flow rate Q (in fact, after the flow collapse, the flow is choked) and Reynolds number.
   The sub cases to be studied were decided starting from the information obtained from figure 5.5. Three main sub cases were considered (listed according to the p_{e2} value): tube completely open with no oscillations (par. 5.4.1),tube with large oscillations (par. 5.4.2) and tube collapsed without oscillations (par. 5.4.3).
   In figure 5.8 it is possible to see that the points considered for the experiments with $p_u = const$ are almost the same than the one studied during the tube's characterization test with the second value of resistance. This makes sense because the aim of the characterization test was to decide the cases to be studied.

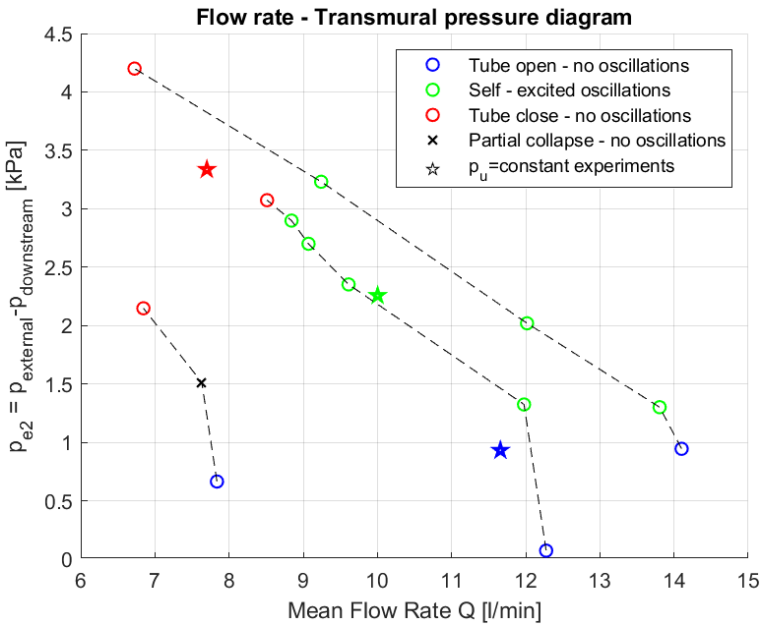

Figure 5.8: Comparison between the cases studied in the final experiment with constant $p_{upstream}$ (stars) and the ones considered in the tube's characterization test (circles).

2. $p_{e2} = const$ **experiments**
   In the last set of experiments the value of $p_{e2} = p_{external} - p_{downstream}$ was kept constant and the flow rate Q was increased (reducing the upstream resistance). It was chosen to kept constant this parameter instead of $p_2 = p_{downstream}$ because, according to the literature, it is more significant the pressure difference between inside and outside of the tube than the absolute value of the pressure. This time, only two sub cases were studied: in the first one the tube was collapsed and there were no oscillations (par. 5.4.4), in the second one the Reynolds number was increased and the oscillations appeared (par. 5.4.5).
   It is important to notice that the open case was not studied because it was not obtainable. The reason is that, once that the oscillations appear because the Reynolds number increases, they lead to flow rate limitation and the flow rate turns to be independent from the pressure upstream. So it is not possible to have the case with a Reynolds number high enough not to have oscillations with the setup used.

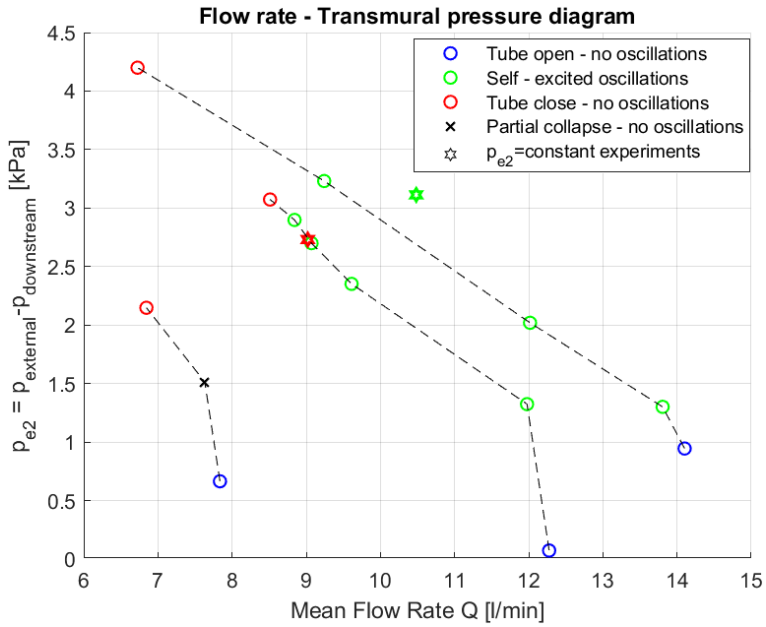

Figure 5.9: Comparison between the cases studied in the final experiment with constant p_{e2} (hexagons) and the ones considered in the tube's characterization test (circles).

5.4.1 Pu constant - Tube open without oscillations

This case has partially been discussed in the paragraph 5.3. In this case, the collapsible tube is completely open even if the transmural pressure is positive (i.e the external pressure is greater than the pressure inside the tube), the flow is laminar and no oscillations are seen neither in the PIV flow field nor in the shape of the tube.

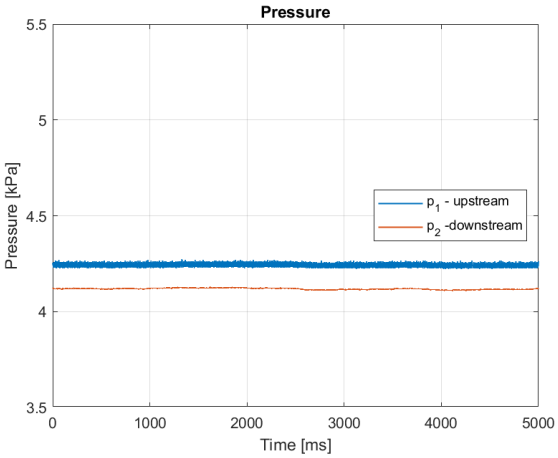

Parameter	Unit	Value
$\overline{Q}$: flow rate	l/min	11.7
v: viscosity	cSt	17
Reynolds number	/	574
$\overline{p_e}$: external pressure	kPa	5.33
$\overline{p_{e2}}$: transmural pressure	kPa	1.22
$\overline{p_1}$: upstream pressure	kPa	4.24
$\overline{p_2}$: downstream pressure	kPa	4.11

Figure 5.10: Pressure diagram (left) and parameters table (right)

Looking at 5.10 the temporal behavior of the pressures p_1 (just upstream of the collapsible tube) or p_2 (just downstream), it is possible to notice that they are constant. The pressure downstream is slightly less than the upstream one because the flow is moving in that direction.

Only figure 5.11 shows the shape of the tube because it does not change. In the figure the colors represent the depth in the y-direction (orthogonal to the page). As it is possible to see, the cross section is circular and the tube is completely open. It is important to remember that the plane of the PIV (x-y plane) and the plane of the Stereo Motion Tracking (x-z plane) are perpendicular (see figure 3.8).

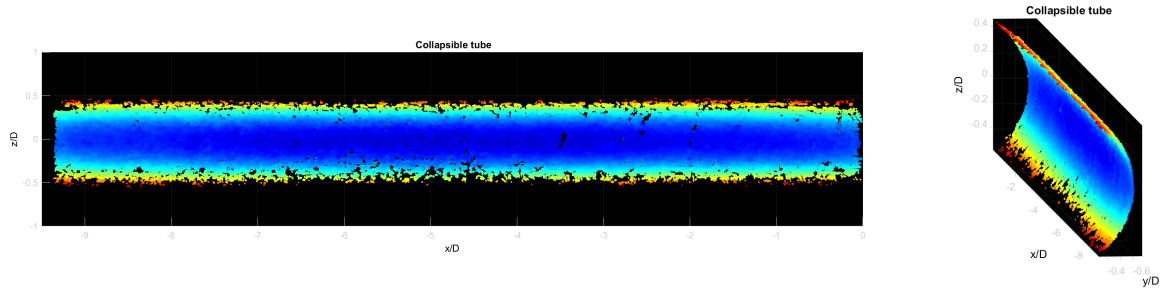

Figure 5.11: 3D reconstruction of the collapsible tube's shape using SMT

5.4.2 Pu constant - Oscillations

In this case the external pressure was increased keeping constant the upstream resistance. As it is possible to notice from figure 5.12, while the upstream pressure p_1 is almost constant, the downstream one p_2 is oscillating periodically. The period of the oscillations is $T = 1.14$ s, that correspond to a frequency of $f = 0.88$ Hz.
The main fluid dynamics parameter of the experiment are:

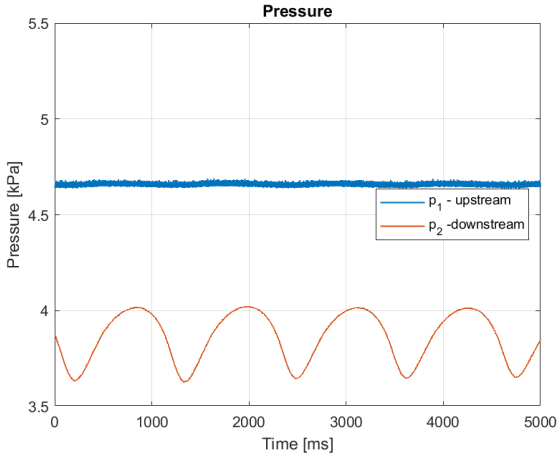

Parameter	Unit	Value
Q: flow rate	l/min	10.0
v: viscosity	cSt	17
Reynolds number	/	491
p_e: external pressure	kPa	6.40
p_{e2}	kPa	2.54
p_1: upstream pressure	kPa	4.66
p_2: downstream pressure	kPa	3.86

Figure 5.12: Pressure diagram (left) and parameters table (right)

In the following analysis, only one oscillation cycle is considered, and non-dimensional time is defined as $\tau = t/T$. Eight different instants are investigated, marked by vertical black lines in figure 5.13, which presents the downstream pressure. Figure 5.14 presents the results of PIV and SMT for these instants.

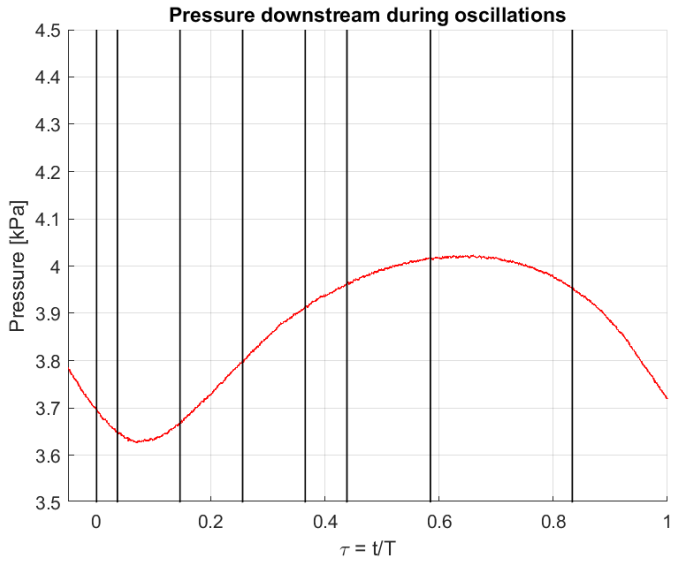

Figure 5.13: Pressure just downstream of the collapsible tube during the self excited oscillations. The vertical black lines represent the instants examined in figure 5.14

In the first two figures ($\tau = 0$ and $\tau = 0.04$) the pressure is decreasing. In particular, for $\tau = 0$, p_2 is close to the minimum one and the tube has its stronger collapse: the

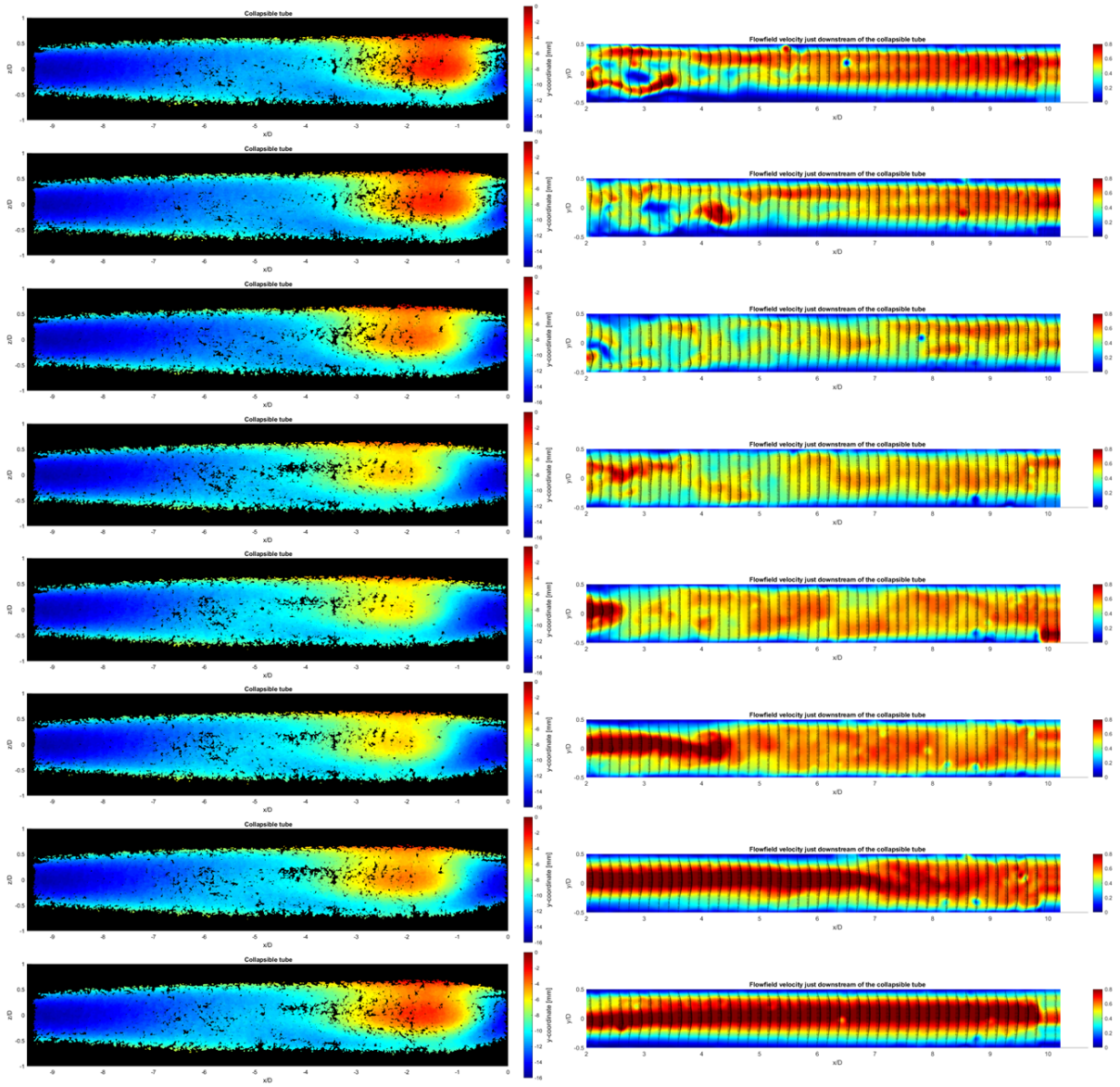

Figure 5.14: stereo motion tracking (left) and PIV results (right). Only one vector every ten in the x-direction is shown in the PIV image. The color map indicates the magnitude of the velocity $|\overline{V}|$ in [m/s]. The instants considered are $\tau = t/T = 0$, 0.04, 0.15, 0.25, 0.37, 0.44, 0.58, 0.83.

collapsed region is the biggest of the entire cycle it has just moved slightly downstream. It was decided to study this case because it is the first instant where it is possible to see that in the upstream portion of the PIV's pipe the flow field starts to oscillate. In fact, up to that moment the flow filed inside the pipe was parabolic and frozen. In particular, it is possible to notice the presence of a vortex in the bottom part of the tube. In the central and right parts of the pipe the flow field is still parabolic.

The second instant considered ($\tau = 0.04$) is very close to the first one, and it is chosen because p_2 reaches the lowest value.
In the PIV image it is possible to notice that the vortex present in the upstream part of the pipe is conveyed downstream by the flow. Its center passed from $x/D \approx 3.5$ (at $\tau = 0$) to $x/D \approx 4.3$ (at $\tau = 0.04$). In the very left part of the pipe, a new vortex with opposite vorticity than the older one is appearing.

After reaching the point with lower p_2, that essentially coincides with the stronger and more downstream collapse of the tube, p_2 starts to increase ($\tau = 0.15$ and $\tau = 0.26$) and and the collapse of the tube starts to weaken (i.e. the y-coordinates of the collapsed portion is further to zero). The collapse is also moving downstream.
Meanwhile, the region with parabolic flow field is moved upstream and almost the entire flow field is dominated by alternate vortexes.

When $\tau = 0.37$ the collapse is the weakest of the cycle and, even if p_2 is still increasing, its concavity has just changed. The most important fact to notice in the PIV results is that in the very upstream portion of the pipe there is a peak of the velocity magnitude and that the velocity profile in that region is getting closer to the parabolic one. In the downstream part of the pipe the vortexes are not distinguishable any more because they are mixed together.

In the following two instants considered ($\tau = 0.44$ and $\tau = 0.58$), the throat of the collapsible tube is mowing forward and the collapse is getting stronger.
It is clearly visible that the region with parabolic flow is moving towards the right portion of the pipe following the main flow.
An important aspect to be considered is that the tube takes more time to collapse ($\Delta\tau \approx 0.6$) than to return to the non deformed shape ($\Delta\tau \approx 0.4$).

In the last instant considered ($\tau = 0.83$) p_2 is almost the maximum one and it is starting to decrease. The Tube is highly collapsed and the region of the collapse is close to the right end of the collapsible tube. Inside the tube the flow field seems frozen and the velocity profile is parabolic. It reminds the case studied in par. 5.4.1.

An important aspect to highlight in this case is the periodicity of the tube oscillations, which is clearly evident in Figure 5.12, where the downstream pressure displays a periodic behavior. Additionally, to further demonstrate this periodicity, we tracked specific points in the flow field, as illustrated in Figure 5.15. We computed the velocities of these points using PIV and then performed a fast Fourier transform (FFT) analysis to identify the main frequencies of oscillation in the velocity.
The results of this analysis are presented in Figure 5.16, which confirms that the main frequency of oscillations in the velocity ($f = 0.88Hz$) is consistent with the frequency

obtained from the pressure data.

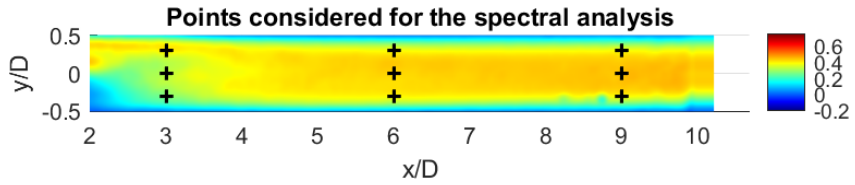

Figure 5.15: Points examined in the PIV's pipe just downstream of the collapsible tube to perform an FFT analysis of the velocity are marked with a black cross

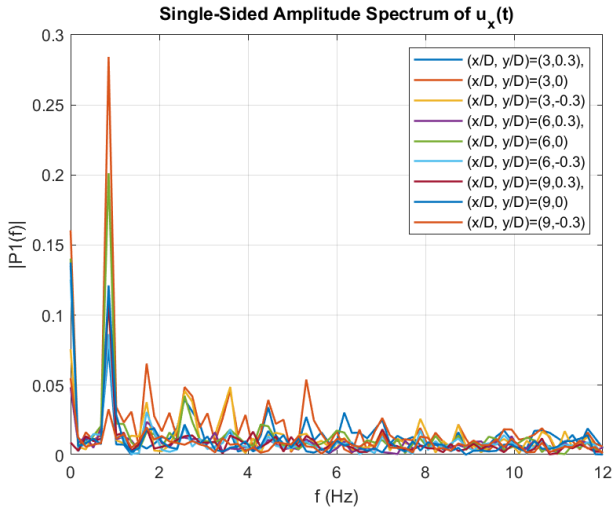

Figure 5.16: Fast Fourier Transformation applied to u_x in the points marked with a cross in figure 5.15

5.4.3 Pu constant - Tube collapsed without oscillations

The last case examined is when the external pressure is high enough to have a complete collapse of the tube without oscillations. In this case the flow inside the collapsible tube is choked.
As it is possible to see from figure 5.17, both the upstream and downstream pressures are constant. Compared to the cases of par. 5.4.1 and 5.4.2, the upstream pressure is the highest and the downstream is the lowest. This means that the pressure drop along the collapsible tube reaches the maximum value.

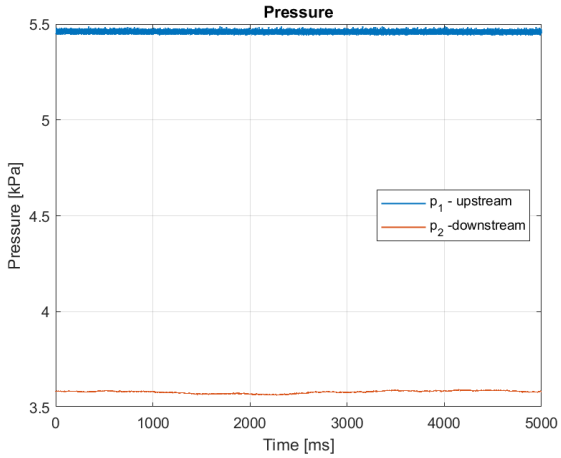

Parameter	Unit	Value
$\overline{Q}$: flow rate	l/min	7.7
v: viscosity	cSt	16
Reynolds number	/	402
$\overline{p_e}$: external pressure	kPa	7.20
$\overline{p_{e2}}$: transmural pressure	kPa	1.74
$\overline{p_1}$: upstream pressure	kPa	5.46
$\overline{p_2}$: downstream pressure	kPa	3.58

Figure 5.17: Pressure diagram (left) and parameters table (right)

One of the primary attributes characterizing the flow field immediately downstream of the collapsible tube is its unsteadiness, as the flow field exhibits neither steadiness nor periodicity.

Figure 5.18 depicts a color map of the velocity magnitude $|\overline{u}|$, where the x-component of the velocity is not always positive throughout the experiment. As such, the regions where $u_x < 0$ are identified by green lines. Ten time instants were considered in the figure, with a total duration of 1.2 seconds. Compared to the cases studied in paragraphs 5.4.2 and 5.4.5, this corresponds to over one cycle. The chosen Δt is sufficiently small to track the flow evolution.

During the experiment, the flow field in the PIV pipe can be divided into three distinctive regions. The first section, extending from $2 < \mathrm{x/D} < 4$, exhibits high u_x at y/D>0 (i.e., the left part of the pipe) and low or negative u_x at y/D<0. The second section, spanning from $4 < \mathrm{x/D} < 7$, displays mixed properties that are difficult to classify. Finally, the third section depicts eddies that have become indistinguishable due to their coalescence. For instance, it is possible to track the evolution of a vortex located at the coordinate (2.5,0.1) at $t = 0$s. The vortex moves downstream and remains visible until t=0.375s, where it reaches the coordinate (3.5,-0.1). Even at this point, the vortex remains distinguishable. By t=0.500s, the vortex has migrated further downstream to the coordinate (4.2, 0.1), although it is less visible than before. Beyond t=0.625s, the vortex becomes too blurred to identify.

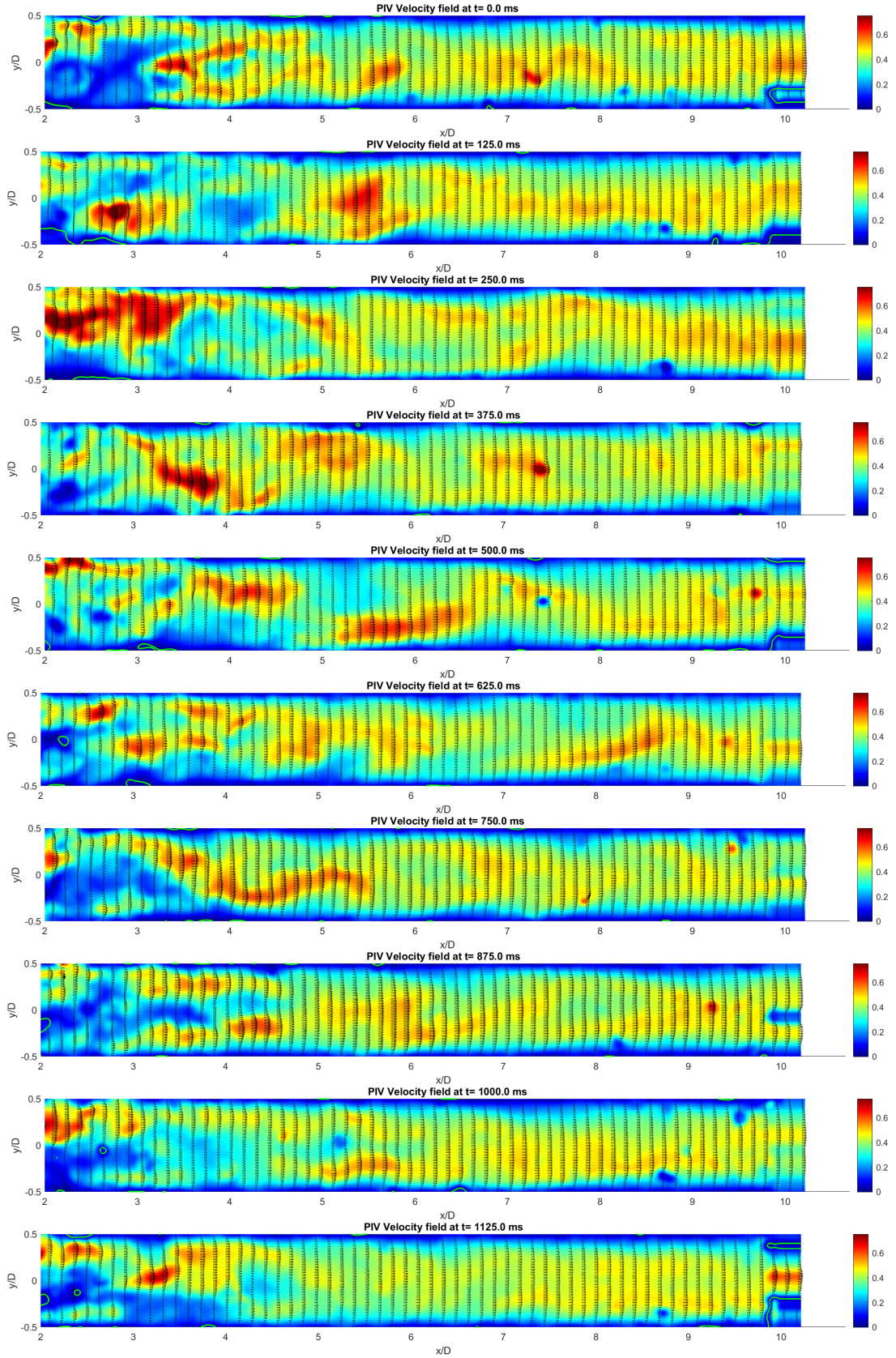

Figure 5.18: PIV velocity field. Only one vector every ten in the x-direction is shown. The color map indicates the x component of the velocity u_x in [m/s]. Ten instants are considered with a time step $\Delta t = 0.125s$

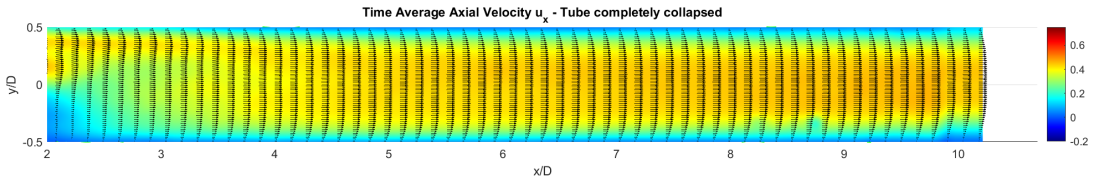

Figure 5.19: PIV images just downstream of the tube in the collapsed case. The color map shows the x component of the velocity, u_x

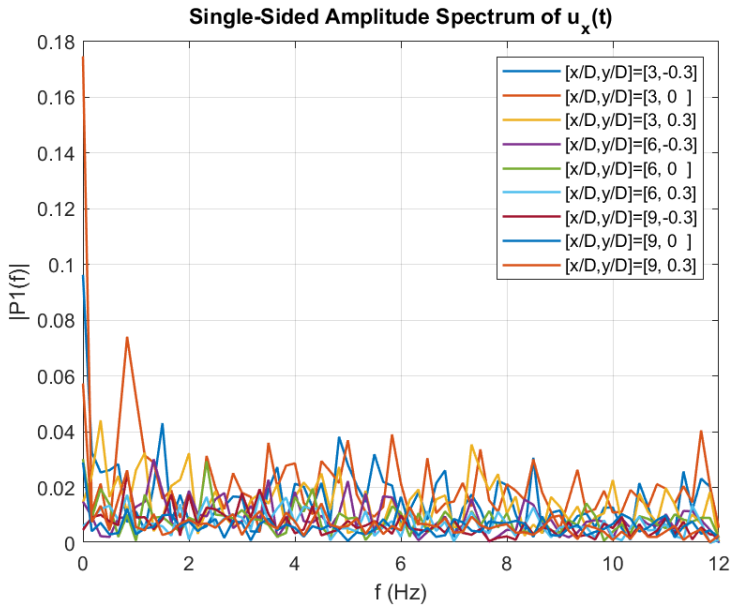

Figure 5.20: Fast Fourier Transformation applied to u_x in the points marked with a cross in figure 5.15

An alternative way to demonstrate the higher velocity of the flow for y/D > 0 in the first section of the pipe is to refer to image 5.19, which presents the time-averaged velocity in the x direction. Throughout the pipe, except for the left segment, the flow field is largely homogeneous. However, the left part of the pipe displays a distinct contrast between the upper and lower portions. By computing the time average of the velocity, the contribution of the different vortices can be averaged out.

Figure 5.20 provides an FFT analysis of the velocity field at fixed PIV pipe coordinates, encompassing the entire domain. The absence of a dominant frequency in the velocity field indicates its chaotic nature. While a frequency of approximately $f \approx 1$ demonstrates the highest magnitude in the figure, it is solitary, with peaks at various frequencies in the other considered coordinates. Comparing these FFT analyses with those of case 5.4.2 reveals that the latter displays a clear dominant frequency.

Only one figure (5.21) of the collapsed tube is presented because the shape is steady. The collapse of the tube happens at the right end of the tube, in the same location than in the oscillating case, considering the instant when the collapse is the stronger.

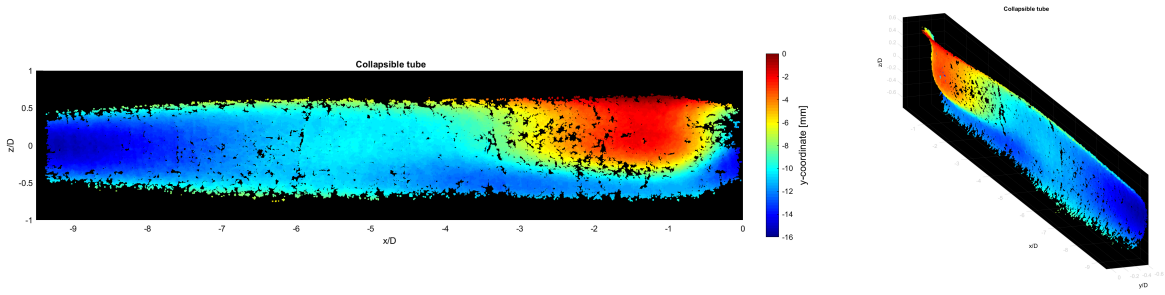

Figure 5.21: 3D reconstruction of the collapsible tube's shape using SMT

5.4.4 Pe2 constant - Tube collapsed without oscillations

The second group of cases considered is characterized by $p_{e2} = p_{external} - p_{downstream} = const$ and the flow rate inside the tube is changed. Between the previous experiment and this one the collapsible tube has been removed to get rid of some bubbles that were disturbing the PIV acquisition and than it was placed again in the same position.

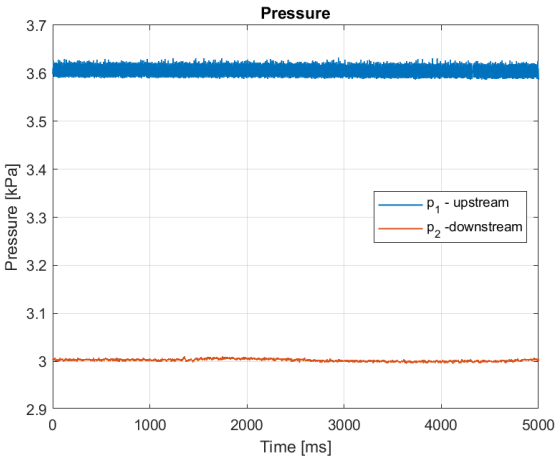

Parameter	Unit	Value
$\overline{Q}$: flow rate	l/min	9.02
v: viscosity	cSt	17
Reynolds number	/	443
$\overline{p_e}$: external pressure	kPa	5.73
$\overline{p_{e2}}$: transmural pressure	kPa	2.73
$\overline{p_1}$: upstream pressure	kPa	3.61
$\overline{p_2}$: downstream pressure	kPa	3.00

Figure 5.22: Pressure diagram (left) and parameters table (right)

From figure 5.22 it is possible to see that both the transducers record constant pressures. The pressure upstream is 0.6 kPa higher than the downstream one. This makes sense because the flow rate is flowing from left to right.

In figure 5.23 is shown the shape of the tube. This case is the only one where the collapse of the tube is not in the downstream end of the tube but at its center. The center of the collapse is at x/D=-4 instead of -2.5<x/D<-1.5 of cases at par. 5.4.2 and 5.4.3. The collapsed reagion is wide but the collapse is weak because the opposite halves of the tube are not completely closed, as happened in case 5.4.3.
This case also differs from the others because the center of the collapse is at z/D=0 and not for z/D>0 (i.e. in the upper part of the tube).

The flow field inside the tube appears to be steady and exhibits a nearly parabolic profile across the pipe cross-section. Figure 4.24 displays the time-averaged velocity field, which is essentially frozen, as the velocity profile does not vary with the x-coordinate. However, there is a spurious low-velocity region in the southeast portion of the pipe that results from

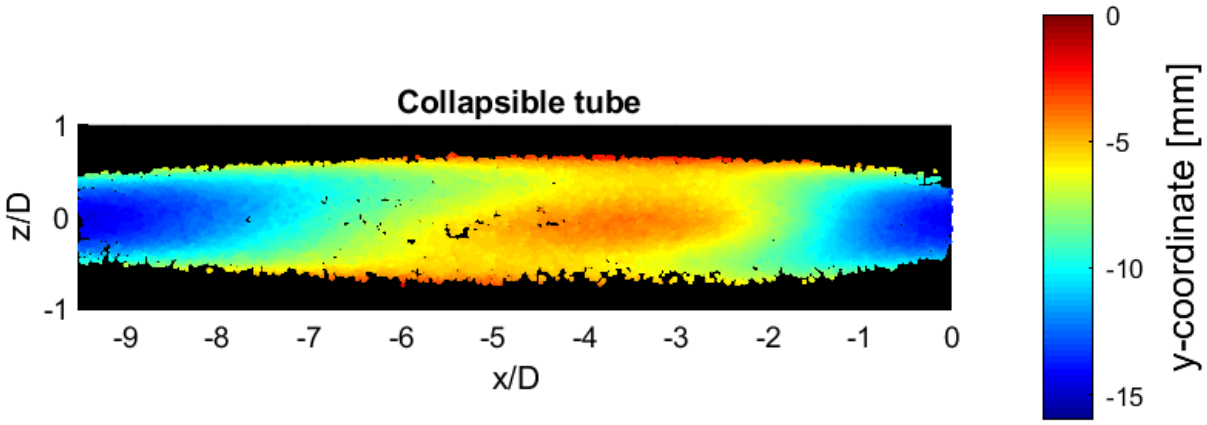

Figure 5.23: 3D shape of the tube obtained applying Stereo Motion Tracking technique

the laser reflection, rather than a physical flow feature. Notably, this case is intriguing because, unlike the fully collapsed configuration (as in case 4.4.3), the flow field lacks any oscillations (as observed in case 4.4.1).

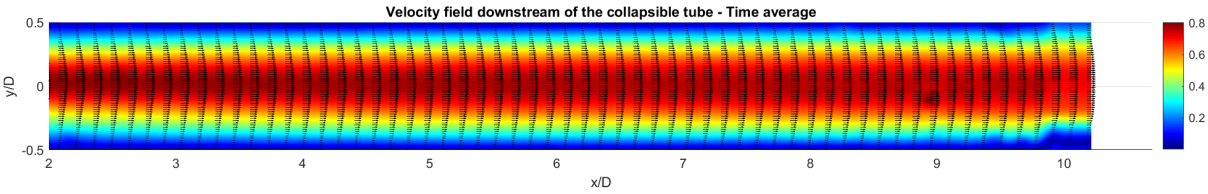

Figure 5.24: PIV results just downstream of the collapsible tube. The color map shows the time averaged velocity magnitude in [m/s]. Only one vector every eight in the x-direction is shown

5.4.5 Pe2 constant - Oscillations

In the last case considered oscillations appeared. Starting from the condition of case 5.4.4, the upstream pressure p_u was gradually incremented, adjusting continuously the external pressure to keep p_{e2} as constant as possible. The increment of the upstream pressure p_u determined an increment of the flow rate. When the flow rate was high enough to have enough kinetic energy inside the collapsible tube, the tube started to oscillate. The following case represent the case with the lowest Reynolds number that allowed wide self-excited oscillations, also called Re_{cr}.

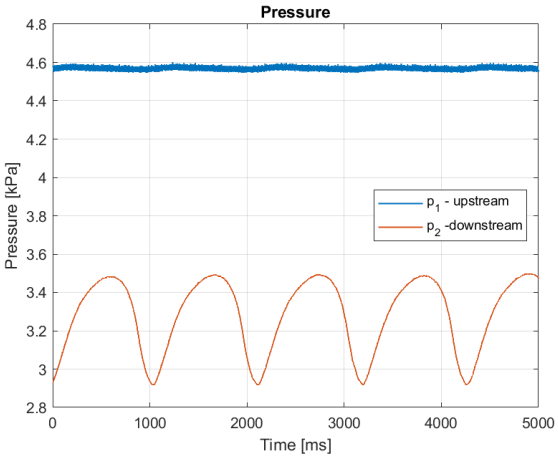

Parameter	Unit	Value
$\overline{Q}$: flow rate	l/min	10.48
v: viscosity	cSt	17
Reynolds number	/	515
$\overline{p_e}$: external pressure	kPa	6.40
$\overline{p_{e2}}$: transmural pressure	kPa	3.12
$\overline{p_1}$: upstream pressure	kPa	4.57
$\overline{p_2}$: downstream pressure	kPa	3.29

Figure 5.25: Pressure diagram (left) and parameters table (right)

As in the other oscillating case presented (par. 5.4.2), the pressure diagram (fig. 5.25) shows that the only pressure that is actually changing is the downstream one, while the upstream pressure is almost steady. The downstream pressure is lower than the upstream one, and the pressure difference $p_{12} = p_1 - p_2$ is greater than in the one in paragraph 5.4.4. The period of the downstream pressure oscillations is $T = 1.075$ s, that corresponds to a frequency of $f = 0.93$ Hz.

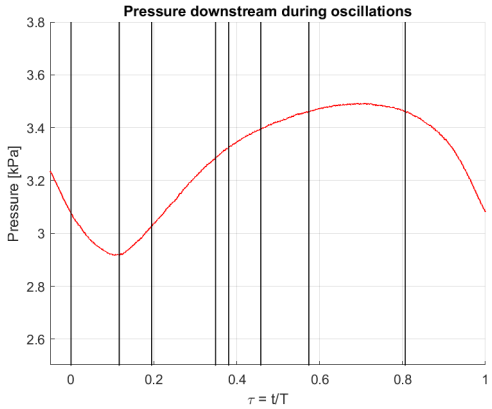

Figure 5.26: Pressure just downstream of the collapsible tube during the self excited oscillations. The vertical black lines represent the instant examined in figure 5.27

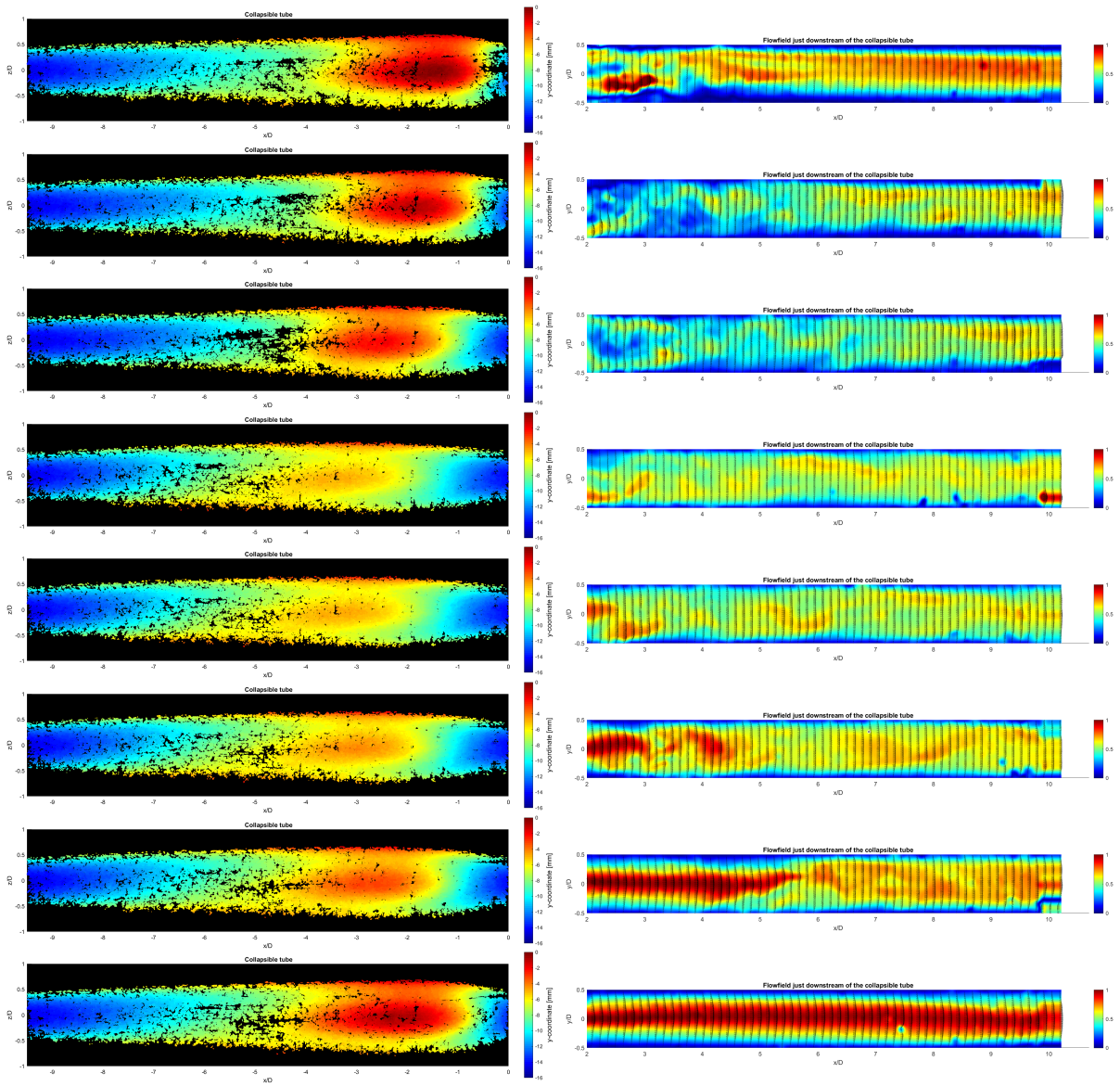

Figure 5.27: stereo motion tracking (left) and PIV results (right). Only one vector every eight in the x-direction is shown in the PIV image. The color map indicates the magnitude of the velocity $|\overline{V}|$ in [m/s]. The instants considered are τ=0, 0.116, 0.194, 0.348, 0.381, 0.458, 0.574, 0.807

In figure 5.27 are shown eight different moments during a cycle. Stereo Motion Tracking and Particle Image Velocimetry are applied to perpendicular planes (see fig. 3.8). The time is divided by the period, calling $\tau = (t - t_0)/T$, where t_0 is the instant of the first image represented and T is the period, in order to obtain more generic results.

As in case 5.4.2, the first instant considered ($\tau = 0$) is the one when the symmetry of the flow field inside the pipe is broken and a vortex with center (2.5, -0.2) is released. Up to that moment, the flow field inside the pipe was parabolic and laminar, similar to the Poiseuille one. Only the upstream portion of the pipe is affected by the symmetry breaking, while downstream portion of the pipe still experiences parabolic velocity profiles. In that instant, the collapse of the tube is the strongest of the entire cycle (shown with the dark red) and its location is at the very end of the tube.

Around τ=0.12 (second image), the lower value of p_2 is reached, the collapse starts to weaken and to move upstream. The vorticity region covers almost half of the pipe ($x/D \sim 5.5$).
The same process of movement of the collapse of the tube towards upstream continues until τ= 0.35 as well as the vortex releasing, when the entire PIV field is dominated by vortexes that have been moved by the flow.

At $\tau = 0.38$ the collapse is the weakest of the cycle and the cross sectional area is the highest. p_2 value is almost the time averaged one and is increasing. p_2 concavity has just changed.
Even if it is possible to locate the center of the collapse at $x/D \sim -3.2$, the partially collapsed region (colored by yellow) is large. The collapse happens for $z/D \sim 0$.
Looking at the PIV's results, it is possible to notice that there are three regions with higher vorticity in the right portion of the domain (that corresponds to the y/D<0), that are located at $x/D \sim 2.8$, $x/D \sim 5.7$ and $x/D \sim 8.1$ (less visible). After each velocity peak in the right part there is one peak in the right side. This leads to an alternating regions all through the pipe.
In the very left portion of the figure there is a peak of the velocity in the axis of the pipe.

Considering the next PIV's image (τ=0.46), it is possible to see that the axial velocity peak is moving downstream following the main flow. The velocity profile in the left region is almost parabolic.
Except for the left region, the properties of the flow inside the pipe have not changed: the vortexes that in the previous figures were all around the pipe have simply moved to the right. For example, the first vortex has moved from $x/D \sim 2.8$ to $x/D \sim 4.3$. During this instant, p_2 is still increasing.
The shape of the collapsible tube is essentially the same of the previous instant considered.

Downstream pressure p_2 reaches almost its maximum value for τ=0.57. Considering the reconstructed surface of the tube, the collapse is starting to be stronger and the center of the collapse is still not moving.
In the left figure, the parabolic core has moved downstream again and it will cover the entire domain at τ=0.80. At that time, the collapse is almost the strongest.

Between the last instant considered (τ=0.80) and the first one of the next cycle (τ=1,

that corresponds to τ=0 of the next oscillation) p_2 drastically decreases and the strongest collapse of the tube is achieved. The collapsed region becomes smaller than in the previous cases and the location of its center has the maximum value of x/D.
The last figure of the series represents the initial situation: the cycle is ended, the parabolic velocity profile characterizes all the pipe and a perturbation of the flow field is going to appear.

The periodic nature of the process can be further elucidated by examining Figure 5.28, which displays the results of Fast Fourier Transform (FFT) analysis performed on the axial component of velocity measured at various locations (indicated in Figure 5.15). The figure reveals that all considered measurement points exhibit identical peaks, indicating the existence of a dominant frequency and its harmonics.

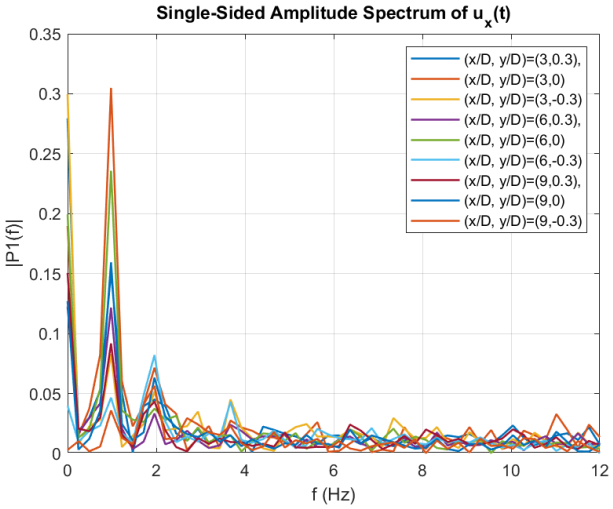

Figure 5.28: Fast Fourier Transformation applied to u_x in the points marked with a cross in figure 5.15

Chapter 6

Discussion

6.1 Tube Law

From the first experiment it is possible to see that the results are quite close to the one presented by [13]. It is important to notice that the Stereo Cameras were not able to reconstruct the entire surface of the collapsible tube but around 160° in the best cases. For this reason, the cross sectional area value, obtained as the interpolation of the y coordinates along the z-axis, could not be perfect.
Another source of possible errors in the cross sectional area computation is that the face of the collapsible tube opposite to camera was not detected. For this reason, the tube was hypothesized to be symmetric respect to the plane of the collapse (plane x-z).

An additional incongruity observed in the experimental results is that the cross-sectional area for both investigated cases appears to increase with external pressure, contrary to the anticipated reduction as predicted by the literature and the tube law. This discrepancy can be attributed to the tube's bending along the z-axis after reaching a certain pressure threshold, whereby the axis of collapse no longer remains straight and coincident with the z-axis. Moreover, it was not possible to increase the external pressure to the extent reported in the literature, as the apparatus became overly stressed beyond 8 kPa. Luckily, the external pressure needed to obtain the self excited oscillations was 7 kPa in the worst case considered.
Another limitation of this study is the inability to obtain and collect data on partial collapse of the tube. This is due to the fact that the pressure difference required to transition from an open to a partially collapsed tube was lower than the accuracy of the pressure regulator.

The aim of this experiment was not the perfect computation of the cross-sectional area but to have two validations: the first about the behavior of the tube and the second about the reliability of the Stereo Motion Tracking method, and both of them worked in this case.

6.2 Tube characterization

Even if the results obtained in the experiment with only water are qualitatively similar to the literature ones because the cases found are the same (steady open, steady collapsed or oscillations), the non dimensional properties are quite different.

The biggest difference between the cases considered and the literature ones is the Reynolds number at wich the oscillations occur, that is about 30 times higher (13600 instead of 350-500). This behavior has not been totally understood because the only difference between the literature setup and the one of the thesis are the geometrical dimensions, that have been doubled keeping constantall the non dimensional groups. This should not affect the Reynolds number that is non dimensional.

On other hand, the case with the water-glycerin mixture has critical Reynolds number that are very similar to the literature one. It is possible to notice that the critical value of flow rate is basically the same for both the cases.

6.3 PIV validation

The PIV validation experiment (fig. 5.7) revealed that the time-averaged velocity profile closely approximates the Poiseuille's profile, indicating that the flow is laminar and fully developed. This means that the length of the upstream and downstream acrylic pipe are long enough to have laminar flow inside the collapsible tube and that the flow conditioner manufactured was working correctly.
Furthermore, it is observed that the no-slip boundary condition is violated due to the smoothing of the code, causing the velocity to be non-zero even in the portion of the setup where the fluid is not moving: in fact, the velocity of the working fluid that surrounded the PIV pipe in the downstream portion of the acrylic tank is computed to be small but different from zero. This is obviously wrong, because there the flow was not mowing.

The experimental setup encounters various sources of error, including reflections of the laser sheet in certain regions. The application of dark sheets of rubber to almost all acrylic walls of the PIV chamber greatly reduces the reflections, but it is not possible to eliminate reflections from the PIV pipe itself. As a result, a consistent region of unacceptable data located at coordinates (10D, -0.45D) in the downstream part of the tube is observed in all PIV experiments carried out.
One last source of error was identified during the PIV calibration process, where some pins on the calibration plate were not detected by the PIV software, particularly in the downstream end of the pipe. Despite this issue, the PIV software reports an error of less than 3% in the computed velocity.

6.4 Final experiment

In the case with $p_u = const$, the cases to be studied have been chosen to be as closer as possible: in the first experiment the external pressure was just under the critical value of oscillations and the third one was the lower value of external pressure that allowed to have the tube completely collapsed without oscillations.
Another comment that could be done about this case is that, even if the upstream resistance is kept constant, the flow rate changes in the sub cases 5.4.1, 5.4.2 and 5.4.3 because there is no choking (that determines Independence between pressure difference and flow rate) as long as the tube is not collapsed.

Considering the case with $p_{e2} = const$, it is possible to see from figure 5.9 that the collapsed case (red hexagon) is very close to an oscillating case previously obtained. This can be explained saying that there is a degree of hysteresis on the physics, and this is in line with the literature experiments.
In fact, all the circles in the maps are experiments carried out with $p_u = const$. While graph 5.8 is reliable, graph 5.9 is useful only to have an idea of the region that is studied. It would have been better to plot a similar $Q - p_{e2}$ graph also with $p_{e2} = const$.

The range of Reynolds numbers, Re=[402, 543], and external pressure, p_{e2}=[1.22, 3.12] kPa, studied in this research are not extensive since the oscillations occur only under specific conditions. For instance, a case where the upstream pressure, p_u, is constant and the external pressure, p_e, is smaller than the one in a reference case (i.e., "pu constant tube open") will exhibit nearly identical characteristics as that reference case. This is because the specific conditions required for oscillations to occur are not met in this scenario, and thus, the range of Reynolds numbers and external pressures studied can be considered narrow. Additionally, it was determined that studying the cases immediately before and after the transition from one state to another would be more feasible and reproducible than studying the transition itself. This decision was made due to the challenging nature of maintaining and reproducing the precise conditions necessary for the transition to occur.

When examining the results of Stereo Motion Tracking (SMT), it is important to consider the removal of the tube between the first set of experiments where the pressure of the fluid was held constant ($p_u = const$), and the second ($p_{e2} = const$) set for the purpose of eliminating bubbles.
Throughout all the experiments conducted in this study, Particle Image Velocimetry was performed exclusively in the x-y plane, as it was deemed important to understand the flow behavior in the plane of tube collapse. However, to gain a more comprehensive understanding of the underlying physics, it is necessary to study the x-z plane as well. It should be noted that the flow field exhibits a highly three-dimensional nature, particularly when eddies are present. Therefore, a multi-dimensional analysis of the flow field would be beneficial in gaining deeper insights into the physical phenomena under consideration. At this point, it is important to mention that in this particular study, a comprehensive analysis of the perpendicular plane (x-z plane) was not possible due to certain limitations in the experimental setup. Specifically, realigning the laser and the camera to perform measurements in the x-z plane was not feasible within the scope of this study. Nonetheless, the findings obtained from the analysis of the x-y plane provide valuable insights into the complex flow behavior, which is critical in designing and optimizing collapsible tube-based devices.

6.4.1 Pu constant - Tube open without oscillations

In this case, the resistance is very low as evidenced by the negligible pressure drop along the tube compared to the oscillating or collapsed cases. The pressure drop in this scenario is solely attributed to viscous stresses. In figure 5.10, the pressure values exhibit slight fluctuations. These fluctuations could be attributed to actual small variations, signal noise, or a combination of both. It is important to note, however, that the accuracy of the pressure transducers used in the experiments is approximately 0.2 kPa, which is

significantly wider than the magnitude of the observed oscillations.

6.4.2 Pu constant - Self excited oscillations

In the present study, it is noteworthy that an increase in pressure drop along the collapsible tube has been observed, as evident from the analysis of figure 5.12. This can be attributed to an increase in resistance as the cross-sectional area decreases, and in addition, the resistance is found to be non-constant. It is important to note that the oscillations are only apparent in the downstream transducer data, which is consistent with previous literature and theoretical expectations. By comparing the results obtained with those of Figure 5.10, it can be inferred that the oscillations correspond to an increase in upstream pressure and a decrease in downstream pressure, while their average remains almost constant.

In this study, it has been observed that the collapse of the tube is not centered ($z/D \neq 0$), and this may be attributed to the non-symmetrical nature of the collapsible tube. While the thickness of the tube was not directly measured, it is possible that non-homogeneous properties of the silicone could have contributed to the observed non-uniformity in tube collapse. Further investigation is required to determine the exact cause of the non-centered collapse.

It has been observed that the velocity profile of the flow exiting the tube is almost parabolic during the initial stages of tube collapse, while it moves slowly in a backward direction. However, as the degree of tube collapse intensifies, the flow field becomes more complex, characterized by the formation of vortices. These observations highlight the critical role of fluid-structure interaction in determining the dynamics of collapsible tube-based systems. This phenomenon provides a notable example of fluid-structure interaction, as illustrated in Figure 5.14.

6.4.3 Pu constant - Tube collapsed

The non symmetry of the flow in figure 5.21 could be related to a non- symmetric collapse of the tube. The non symmetric collapse was already noticed during the tube law experiments, where the computation of the area was not perfectly fitting with the expectations.

Apparently, the external pressure was not high enough to extinguish completely the oscillations of the flow field, even if the tube's shape was completely steady. It would have been interesting to run another experiment increasing the external pressure again, to determine if the unsteadiness of the flow persists.

Upon comparing the outcomes of the CFD simulation study [12], which considered constant Reynolds number and increased $P_e = p_{e2}/0.5 \cdot \rho \cdot U^2$, with the experimental results presented in this work, it is observed that the magnitude of oscillations between the cases described in paragraphs 5.4.3 and 5.4.2 increases as expected. However, it is important to note that this phenomenon is not consistently observed in the real experimental setup. Specifically, as mentioned in paragraph 5.4.3, the collapsible tube can undergo collapse without any accompanying wall oscillations after a certain threshold is reached. The results obtained from the FFT analysis underlines that the case can be considered

chaotic, adopting the definition of the CFD article [12].

6.4.4 Pe2 constant - tube collapsed

This case is interesting because most of the properties of the system are an hybrid of the previous examined in paragraph 5.4.3 and 5.4.1 . For example, looking at the pressure transducers' data, it is possible to notice that the resistance between the upstream and downstream end of the collapsible tube has a value of $R = \Delta p_{12}/Q = 7.3 \cdot 10^6\ Pa \cdot s/m^3$, with the tube open was $R = 0.67 \cdot 10^6\ Pa \cdot s/m^3$ (par. 5.4.1) and with the collapsed tube $R = 14.6 \cdot 10^6\ Pa \cdot s/m^3$ (par. 5.4.3). In this case, both the upstream and downstream pressure are constant.

The reconstructed shape of the collapsible tube (as depicted in Figure 5.23) exhibits similarities with the fully collapsed scenario, albeit the collapsed section of the tube appears to span a larger region, albeit with lower intensity. It is worth noting that all Stereo Motion Tracking images employ the same color scale. In this instance, it is apparent that the maximum displacement in the y-axis direction is less than 10mm, whereas previous observations have exceeded 12mm. Furthermore, it is noteworthy that no red regions are discernible in this image.

On the other hand, the velocity field in appears to closely resemble the velocity field of the tube in its fully open configuration (case 5.4.1), which is characterized by a parabolic velocity profile throughout the field of view of the PIV camera. The instantaneous velocity field in this instance is remarkably similar to the time-averaged velocity field. However, the decision to present the time-averaged field is driven by the desire for greater generality in the presentation of results.

6.4.5 Pe2 constant- self-excited oscillations

This case is very similar with the oscillating case with constant p_u. Starting from the pressure diagram at figure 5.25, it is possible to see that the only pressure that is significantly changing is the downstream one, as expected from the literature. Not only the shape of the $p_2(t)$ curve but also its frequency of oscillation is similar to case 5.4.2.

Based on the Stereo Motion Tracking results, it is apparent that the collapsed region is larger than that in the $p_u = const$ counterpart and has shifted upstream in comparison. Other than this dissimilarity, the velocity field cycle remains fundamentally the same, exhibiting alternating periods of parabolic laminar flows and high vorticity ones.

Chapter 7

Conclusions

In this study, a novel experimental setup was designed and constructed to investigate collapsible tube dynamics and self-excited oscillations using two optical techniques simultaneously for the first time. The Stereo Motion Tracking technique was utilized to examine the shape of the tube, while Particle Image Velocimetry was used to capture the flow field just downstream of the collapsible tube in two perpendicular planes.

The initial experiments involved gradually increasing the pressure difference p_{e2} while maintaining constant upstream resistance p_u. Three cases were examined: the first with a completely open tube exhibiting steady and laminar flow; the second with self-excited periodic oscillations; and the third with a completely collapsed tube that resulted in chaotic flow, particularly in the downstream region of the tube where the flow was asymmetric. The second set of experiments examined two Reynolds numbers, one below and one just above the critical Reynolds number, with a constant pressure difference p_{e2}. At the lower Reynolds number, the tube was collapsed, and the flow field downstream was steady and parabolic. As the Reynolds number increased, oscillations appeared.

Interestingly, the oscillating cases exhibited similar characteristics despite being obtained through different processes. The oscillation cycle could be divided into two phases: the first phase with low pressure and weaker tube collapse, resulting in an unsteady and vortical flow field; and the second phase with increasing pressure, stronger tube collapse, and a parabolic velocity profile inside the tube. The collapsed cases also exhibited significant differences, with one obtained at constant p_u resulting in chaotic flow, while the other obtained at constant p_{e2} exhibited parabolic velocity profiles. Hysteresis was observed between cases with similar parameters, where one resulted in collapsed flow and the other in oscillating flow.

Although the obtained results are satisfactory, there is room for improvement to further enhance the findings. For instance, volumetric PIV could be performed to obtain a comprehensive understanding of the three-dimensional velocity component, which was neglected in this study. Alternatively, a 2D3C (two-dimensions-three-components) PIV could be considered sufficient. It would also be interesting to investigate the plane perpendicular to the one utilized in this research. Additionally, the bubbles in the pipes were one of the primary limitations of the system, and a suitable technique to remove them efficiently would be beneficial.

Bibliography

[1] C.D. Bertram and J. Tscherry. "The onset of flow-rate limitation and flow-induced oscillations in collapsible tubes". In: *Journal of Fluids and Structures* 22.8 (2006), pp. 1029–1045. DOI: https://doi.org/10.1016/j.jfluidstructs.2006.07.005.

[2] T. J. Pedley C. Cancelli. "A separated-flow model for collapsible tube oscillations". In: *Journal of Fluid Mechanics* (1985).

[3] R. J. Castles C. D. Bertram. "Flow limitation in uniform thick walled collapsible tubes". In: *Journal of Fluids and Structures* (1999).

[4] S. D. Hall C. D. Bertram N. K. Truong. "PIV Measurements of the Flow Field Just Downstream of an Oscillating Collapsible Tube". In: *Journal of Biomechanical Engineering* (2008).

[5] N. K. Truong C.D. Bertram. "The flow-field downstream of a collapsible tube during oscillation onset". In: *Communications in Numerical Methods in Engineering* (2009). DOI: https://doi.org/10.1002/cnm.1226.

[6] A. K. Ouazzane E. M. Laws. "A further study into the effect of length on the Zanker flow conditioner". In: *Flow Meas. Instrum.* (1995).

[7] Xie-Zhen Yin Hai-Jun Wu Lai-Bing Jia. "Experiments on self-excited oscillation in a thin-walled collapsible tube". In: *Acta Mechanica Sinica* (2015). DOI: DOI10.1007/s10409-015-0465-y.

[8] Waters Heil. "How rapidly oscillating collapsible tubes extract energy from a viscous mean flow". In: *Journal of Fluid Mechanics* (2008). DOI: 10.1017/S0022112008000463.

[9] H.T.Low J.W.Wang Y.T.Chew. "Effects of downstream system on self-excited oscillations in collapsible tubes". In: *Communications in numerical methods in engineering* (2009), pp. 429–445. DOI: 10.1002/cnm.1238.

[10] E.M. Laws. "Flow conditioning - A new development". In: *Flow Meas. Instrum.* (1990).

[11] E. Ozahi M. O. Carpinlioglu. "Laminar flow control via utilization of pipe entrance inserts (a comment on entrance length concept)". In: *Flow Meas. Instrum.* (2011).

[12] John Young Qiuxiang Huang Fang-Bao Tian and Joseph C.S. Lai. "Transition to chaos in a two-sided collapsible channel flow". In: *Journal of Fluid Mechanics* (2021). DOI: 10.1017/jfm.2021.710.

[13] A.H. Shapiro. "Steady Flow in Collapsible Tubes". In: *ASME, Journal of Biomechanical Engineering* (1977), pp. 126–147. DOI: https://doi.org/10.1115/1.3426281.

Acknowledgements

Questo lavoro è dedicato alla mia famiglia: Manuel, Barbara, Ivan e Emma.

Ringrazio la Professoressa Stefania Scarsoglio che si è sempre dimostrata competente, gentile e disponibile.